Graduate School Form 30
Updated 1/15/2015

PURDUE UNIVERSITY
GRADUATE SCHOOL
Thesis/Dissertation Acceptance

This is to certify that the thesis/dissertation prepared

By Arash Jamali

Entitled

NUMERICAL SIMULATION OF COMBUSTION AND UNBURNT PRODUCTS IN DUAL-FUEL COMPRESSION-IGNITION ENGINES WITH MULTIPLE INJECTION

For the degree of Master of Science in Mechanical Engineering

Is approved by the final examining committee:

M. Razi Nalim
Chair

Whitney Yu
Co-chair

Likun Zhu
Co-chair

To the best of my knowledge and as understood by the student in the Thesis/Dissertation Agreement, Publication Delay, and Certification Disclaimer (Graduate School Form 32), this thesis/dissertation adheres to the provisions of Purdue University's "Policy of Integrity in Research" and the use of copyright material.

Approved by Major Professor(s): M. Razi Nalim

Approved by: Jie Chen 12/9/2015
Head of the Departmental Graduate Program Date

NUMERICAL SIMULATION OF COMBUSTION AND UNBURNT PRODUCTS IN DUAL-FUEL COMPRESSION-IGNITION ENGINES WITH MULTIPLE INJECTION

A Thesis

Submitted to the Faculty

of

Purdue University

by

Arash Jamali

In Partial Fulfillment of the

Requirements for the Degree

of

Master of Science in Mechanical Engineering

December 2015

Purdue University

Indianapolis, Indiana

To my parents, Mansoureh and Alimardan.

ACKNOWLEDGMENTS

First and foremost, I would like to express my gratitude to Professor Razi Nalim for accepting me into his research group at the Mechanical Engineering Department and being a nice advisor.

I also would like to show my appreciation for all faculty and stuff in mechanical engineering department. In particular, Professors Whitney Yu and Likun Zhu.

Finally I would like to thank Dr. Satbir Singh for sharing more detail of his papers, Convergent Science Inc for donating the CFD code to Combustion and Propulsion Lab at IUPUI and all of my friends and family for their love and support.

TABLE OF CONTENTS

Page

LIST OF TABLES

LIST OF FIGURES

Figure Page

Appendix Figure

ABSTRACT

Jamali, Arash. M.S.M.E., Purdue University, December 2015. Numerical Simulation of Combustion and Unburnt Products in Dual-Fuel Compression-Ignition Engines with Multiple Injection. Major Professor: M. Razi Nalim.

Natural gas substitution for diesel can result in significant reduction in pollutant emissions. Based on current fuel price projections, operating costs would be lower. With a high ignition temperature and relatively low reactivity, natural gas can enable promising approaches to combustion engine design. In particular, the combination of low reactivity natural gas and high reactivity diesel may allow for optimal operation as a reactivity-controlled compression ignition (RCCI) engine, which has potential for high efficiency and low emissions. In this computational study, a lean mixture of natural gas is ignited by direct injection of diesel fuel in a model of the heavy-duty CAT3401 diesel engine.

Dual-fuel combustion of natural gas-diesel (NGD) may provide a wider range of reactivity control than other dual-fuel combustion strategies such as gasoline-diesel dual fuel. Accurate and efficient combustion modeling can aid NGD dual-fuel engine control and optimization. In this study, multi-dimensional simulation was performed using a finite-volume computational code for fuel spray, combustion and emission processes. Adaptive mesh refinement (AMR) and multi-zone reaction modeling enables simulation in a reasonable time. The latter approach avoids expensive kinetic calculations in every computational cell, with considerable speedup. Two approaches to combustion modeling are used within the Reynolds averaged Navier-Stokes (RANS) framework. The first approach uses direct integration of the detailed chemistry and no turbulence-chemistry interaction modeling. The model produces encouraging agreement between the simulation and experimental data.

For reasonable accuracy and computation cost, a minimum cell size of 0.2 millimeters is suggested for NGD dual-fuel engine combustion. In addition, the role of different chemical reaction mechanism on the NGD dual-fuel combustion is considered with this model.

This work considers fundamental questions regarding combustion in NGD dual-fuel combustion, particularly about how and where fuels react, and the difference between combustion in the dual fuel mode and conventional diesel mode.

The results show that in part-load working condition main part of CH_4 cannot burn and it has significant effect in high level of HC emission in NGD dual-fuel engine. The CFD results revel that homogeneous mixture of CH_4 and air is too lean and it cannot ignite in regions that any species from C_7H_{16} chemical mechanism does not exist.

It is shown that multi-injection of diesel fuel with an early main injection can reduce HC emission significantly in the NGD dual-fuel engine. In addition, the results revel that increasing the air fuel ratio by decreasing the air amount could be a promising idea for HC emission reduction in NGD dual-fuel engine, too.

1. INTRODUCTION

Compression ignition (CI) engines have relatively better thermal efficiency than spark ignition (SI) engines, but they are challenged by high NO_X and soot emissions. This is illustrated in terms of local equivalence ratio and adiabatic flame temperature by Kamimoto [1] in Fig. 1.1. In a typical diesel engine, CI engine, there are two distinct zones where combustion and pollution formation occur: a diffusion flame where locally $\phi \cong 1$ and there is high level of NO_X due to high adiabatic flame temperature; and a rich premixed combustion zone where $2 < \phi < 3$ with high levels of soot formation.

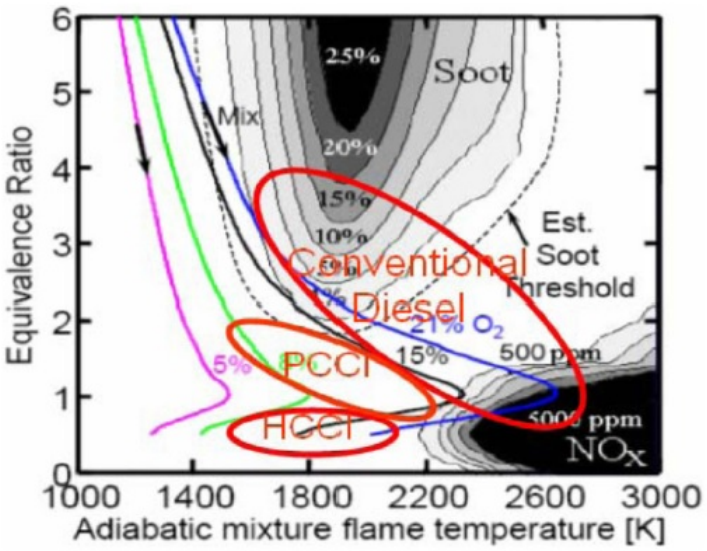

Fig. 1.1. Soot and NO_X formation regions in $\Phi - T$ space. Overlaid are operating regimes of conventional diesel, premixed charge compression ignition (PCCI), and homogeneous charge compression ignition (HCCI) [1, 2]

To reduce pollutant formation, strategies to avoid high combustion temperatures and rich combustion have been investigated. Specifically, low-temperature combustion of lean mixtures can occur with homogeneous charge compression ignition

(HCCI) [3], resulting in very low NO_X and soot emissions Fig. 1.1. However, the HCCI concept faces significant challenges in controllability of the auto-ignition timing and heat release rate (HRR).

These challenges could be overcame by partially premixed compression ignition (PPCI). In PPCI, the major portion of the fuel is injected early in the cylinder, before compression, to have enough time for mixing before ignition. A smaller late injection of fuel, near top dead center (TDC), initiates ignition. Researchers at Lund University [4] have studied different aspect of PPCI strategies. They have found that single-fuel PPCI combustion can yield high thermal efficiency and low emissions. However, keeping an acceptable maximum pressure rise rate is a challenge for PCCI [2, 4].

Improved combustion control can be achieved by using more than one fuel with different reactivity and appropriate injection strategies. Reitz et al. at the University of Wisconsin [5, 6] employed a dual-fuel strategy with a focus on fuel reactivity and named it reactivity-controlled compression ignition (RCCI). The port fuel injection of gasoline, a fuel with low reactivity, and direct injection of diesel fuel, with high reactivity, allowed for better control of the combustion phase. They have found that in-cylinder fuel blending reduces the maximum pressure rise rate compared to single-fuel premixed combustion due to optimized reactivity gradients established in the chamber [2, 6]. They have shown that higher reactivity gradient of fuels can utilize longer combustion duration and reduce pressure rise rate. Natural gas has even lower reactivity than gasoline, suggesting that gas-diesel dual-fuel combustion can also be classified and understood in the RCCI framework.

Natural gas fumigation in heavy-duty diesel engines is commercially attractive today due to its lower price and cleaner burning characteristics that included low CO_2 and NO_X and low soot emissions.

Fig. 1.2 shows the long term availability of natural gas resources in comparison with crude oil resources. The graph shows that the total availability of natural gas (i.e. conventional plus non-conventional resources) is approximately 150% of the

availability of crude oil. It also indicates that the projected consumption of natural gas bound energy from 2013 to 2035 is approximately 25% less than the one from crude oil. Therefore, shifting toward technologies using natural gas will help to balance the projected mismatch of fuels offers and demands.

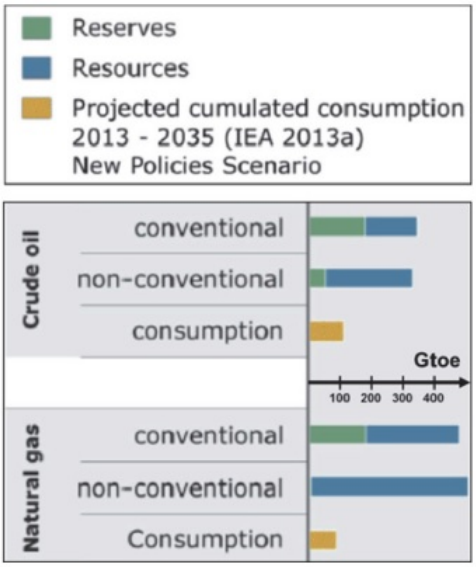

Fig. 1.2. Availability of natural gas in comparison to crude oil [7]

Fig. 1.3 shows the price situation at randomly picked fuel station in different countries from mid-August 2014. It indicates that the compressed natural gas (CNG) price has advantages between 16 to 80 percent in the different countries.

In addition, the simple and low-cost mechanical modification of adding a fuel-gas injection system in the existing intake manifold of diesel engines allows flexible-fuel operation with easy reversion to conventional diesel operation in backup mode. This type of gas-diesel dual fuel engines [8] has been experimentally investigated and commercialized before the RCCI concept.

For greatest benefit, the fumigated gaseous fuel will provide most of the input energy, with diesel serving as the faster igniting pilot fuel. The quantity of pilot fuel should be as small as necessary to ensure timely and complete combustion, without decreasing the thermal efficiency or increasing the amount of the unburned hydrocar-

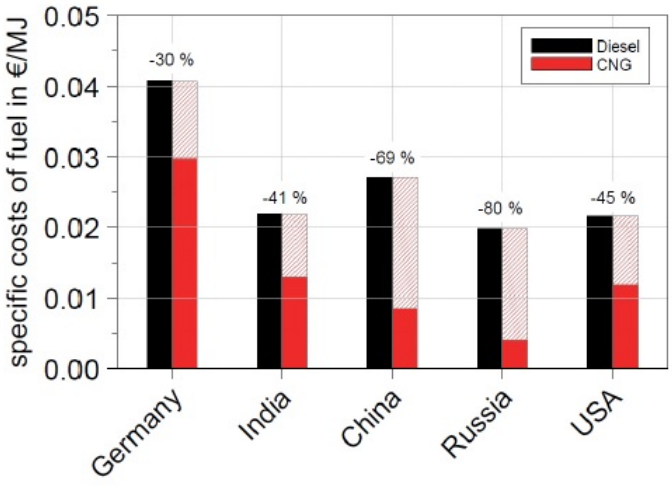

Fig. 1.3. Comparison of fuel cost per energy content in different markets.(The prices in the figure reflect the uneven offer and demands and the related fuel taxes in the different countries.) [7]

bons [9,10]. Another characteristic of NGD dual-fuel engine is that the peak pressure rise rate is relatively low because of the high reactivity gradients between diesel and natural gas in comparison with single-fuel or other dual-fuel concepts such as gasoline-diesel dual-fuel and PCCI engine.

1.1 Modeling Approaches in Dual-fuel Engine

Most prior research on NGD dual-fuel engines focused on thermodynamic modeling and engine experiments. Deeper investigation of the combustion process is necessary, especially for improving emission control and engine performance. The goal of this work is to accurately simulate the flow dynamics in NGD dual-fuel engine and then provide some suggestion to improve the performance of NGD dual-fuel engine based on the detailed CFD results.

Liu and Karim [11] simulated the thermodynamic process of the gas-diesel dual-fuel engine and predicted HRR using a five-zone combustion model with double-Weibe

function [12, 13]. Hountalas and Papagiannakis [14] used a combustion model with two zones - burned and unburned. Furthermore, experimental studies have examined parameters such as diesel fuel quantity, and timing on combustion efficiency and pollutants of NGD dual-fuel engines [10].

Much of the research [9, 10]indicates lower NO_X and soot emissions but higher carbon monoxide (CO) and total hydrocarbons (THC) emissions in NGD dual-fuel mode, in comparison with conventional diesel mode. Liu et al. [9] showed that (THC) emitted increases significantly with decrease of the pilot diesel quantity.

Multidimensional CFD modeling considers spatial and temporal development of the physical and chemical processes of combustion, and can include complex phenomena, such as turbulence to provide predictive results useful for engine control and emission reduction. Zhang et al. [15] simulated a NGD dual-fuel engine with multidimensional CFD based on the Shell chemical autoignition model (used for relatively lower temperature regions) and the characteristic time combustion (CTC) model [16]. They calibrated some constants in the CTC model to predict pressure and HRR in a NGD dual-fuel engine, and validated the model for two heavy-duty diesel engines. Singh et al. [17] showed that the model of Zhang et al. fails to predict experimentally measured HRR when the amount of energy that comes from gaseous fuel is more than 90% of the total energy. This combustion model is not inherently an adequate predictive model as it requires tuning many constants [18]. Singh et al. developed a flame propagation model for NGD dual-fuel engines when more than 90% of the total energy available is from natural gas [19]. In this model, the Shell autoignition model was used to predict the ignition of diesel fuel and the formation of the ignition kernel. As soon as an ignition kernel was formed, further combustion by flame propagation is modeled by a level-set model using a scalar variable G that has a prescribed value within the flame [20].

1.2 Problem Formulation

In this study, multidimensional CFD was coupled with a detailed chemical mechanism to predict the combustion in a fuel-lean NGD dual-fuel engine. Whereas mixtures richer than an equivalence ratio of 0.6 are expected to support flame propagation and they are not considered in this research. However, the equivalence ratio that combustion of NGD dual-fuel engine begins to exhibit flame propagation behavior is not well defined, given that the limited research used different engines and conditions.

The simulation was conducted for a Caterpillar 3401 diesel engine operated at part load (40% load, 21 kW) with no EGR (exhaust gas recirculation) and turbocharged operation. The schematic of the test case is shown the following Fig.1.4.

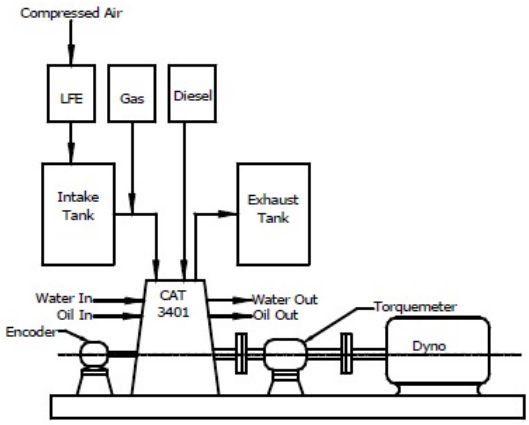

Fig. 1.4. Schematic of the test engine setup

All the CFD cases in this work are build based on experimental data and information given by Singh et al. [17] and additional information which is attached in Appendix.A here. As shown in the above figure, natural gas is injected into the intake port, and mixes with air during the induction stroke. The homogeneous natural gas-air mixture, with an estimated equivalence ratio of 0.2 is then compressed without reaching auto-ignition conditions and is ignited by the injection of liquid diesel fuel near top dead center (TDC). Engine parameters considered for the computational analysis are summarized in Table 1.1, and are given by Singh et al. [17].

Table 1.1.
Engine Specification

Engine model	Caterpillar-3401
Bore and stroke (mm)	137.16 and 165.1
Displacement volume (L)	2.44
Compression ratio	15.1:1
Number of injection nozzles per cylinder	6
Nozzle diameter (mm)	0.26
Piston type	Mexican Hat
Injection system	Common rail
Rated Power (kW)	52 @ 2100 rpm
Fuel Injection	Direct Injection

The simulation includes the physial processes of the compression, direct injection of liquid fuel, combustion, and expansion inside the cylinder. As the intake and exhaust processes were not simulated, the valves have been omitted from the model. The injector consists of six equally spaced fuel nozzles. Assuming rotational periodicity, a 60-degree sector of the cylinder including a single spray nozzle is simulated (Fig. 1.5). It is noted that fuel and combusting gas transported from one sector to the next is accounted for by the periodic boundary conditions.

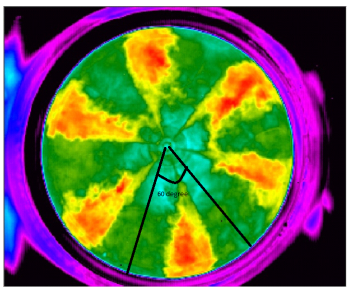

Fig. 1.5. Top view of the thermal spectrum of diesel engine combustion.

2. MODELING APPROACH

In the current study, the CFD code $CONVERGE^{TM}$, Version 2.1 [21] provided a finite-volume methodology capable of handling complex three-dimensional geometries with moving boundaries, transient liquid sprays, turbulence, and detailed chemical kinetics. The transport equations; mass, momentum, species and energy equations; are solved using the pressure-implicit method with splitting of operators (PISO). Turbulence is modeled using the standard renormalization group (RNG) $k-\epsilon$ turbulence model. Adaptive mesh refinement (AMR) and multi-zone chemistry computation are used to maximize the resolution of important features and to minimize the numerical cell count and kinetics calculation times. Detailed kinetic modeling is performed using the SAGE chemical kinetic solver, which is coupled with the CFD code. More details about AMR and the combustion model are provided in the following sections.

In this study, predictions from simulation are compared with experimental data from Singh et al. [17], specifically pressure traces and HRR estimated therefrom. Natural gas chemical mechanism is represented by pure methane (CH_4) and diesel by n-heptane (C_7H_{16}) for simplicity. These surrogate fuels have similar chemical behavior to the real fuel, which is generally variable in composition. It is acknowledged that higher hydrocarbons in natural gas can accelerate reaction rates and influence important phenomena, such as pressure oscillations. Two chemical kinetic mechanisms are evaluated for combustion of methane and n-heptane: the more complete 76-species 464-reactions mechanism [22] and a shorter 29-species 54-reactions mechanism [2, 23]. It is assumed that the methane and air mixture is homogeneous at the start of the simulation immediately after the inlet valve closes.

2.1 Detailed Chemistry Without Turbulence-chemistry Interaction (SAGE kinetics solver)

This model assumes relatively slow chemistry in comparison with turbulent mixing rates, such that each computational cell is well-mixed. Chemical reaction rates are computed using the SAGE solver [24] which is coupled to the CFD solver. The code accepts CHEMKIN-formatted chemical reaction mechanisms. The chemical reaction rates are computed for each computational cell based on temperature, pressure, and species mass fractions at the start of each time step, and the species mass fractions are then updated.

A reaction mechanism can be written as:

$$\sum_{m=1}^{M} \nu'_{m,r}\chi_m \Longleftrightarrow \sum_{m=1}^{M} \nu''_{m,r}\chi_m \qquad for\ r = 1, 2, ...R \tag{2.1}$$

Here R is the total number of reactions and χ_m is the chemical symbol of species m. $\nu'_{m,r}$ and $\nu''_{m,r}$ are the stoichiometric coefficients of reactants and products respectively for species m and reaction r. The net production rate can be calculated from:

$$\dot{\omega}_m = \sum_{r=1}^{R} \nu_{m,r}\zeta_r \qquad for\ m = 1, 2, ...M \tag{2.2}$$

Where M is total number of species, ζ_r is rate-of-progress variable and

$$\nu_{m,r} = \nu''_{m,r} - \nu'_{m,r} \tag{2.3}$$

ζ_r can be calculated from

$$\zeta_r = k_{fr} \prod_{m=1}^{M} [X_m]^{\nu'_{m,r}} - k_{br} \prod_{m=1}^{M} [X_m]^{\nu''_{m,r}} \tag{2.4}$$

Here k_{fr} and k_{br} are forward rate coefficient and backward rate coefficients respectively for reaction r. $[X_m]$ is the molar concentration of species m. The forward and backward rate coefficients can be written in Arrhenius form:

$$k_{fr} = AT^{b}exp^{(-E_A/R_uT)} \tag{2.5}$$

Here A is a constant named pre-exponential factor, b is temperature constant, E_A is activation energy and R_u is universal gas constant. The backward rate coefficient can also be calculated from equilibrium coefficient calculations. A, b and E_A are given in a reaction mechanism for each elementary reaction.

Sub-grid scale turbulence chemistry interaction (TCI) is not considered in this model [25]. The accuracy of this model is highly dependent on the mesh size, especially in the flame front area.

To reduce the chemical computation time, a multi-zone method is used. The chemical kinetics in each computational cell is solved in zones, i.e. groups of cells that have similar thermodynamic state [26].

2.2 The Representative Interactive Flamelet (RIF) Model

The Representative Interactive Flamelet (RIF) model is introduced to count the effect of the sub-grid scale TCI in chemical kinetic calculation. The Representative Interactive Flamelet (RIF) model was originally situated for non-premixed combustion regime. The concept of RIF model is based on the laminar flamelet equations and assumption that reaction zone is thin and width of it is much smaller than characteristic length scale of turbulent eddies [26]. The flamelet approach is based on idea that turbulent flames are ensemble of instantaneous flame fronts as shown in Fig. 2.1.

One of the important principles in flamelet approach relies on a conserved scalar which is called mixture fraction, Z, and is defined as follows:

$$Z = \frac{m_f}{m_f + m_o} \tag{2.6}$$

where m_f is mass flux coming from fuel stream and m_o is the mass flux coming from oxidizer stream. As shown in Fig.2.2 the value of Z is zero in oxidizer side and

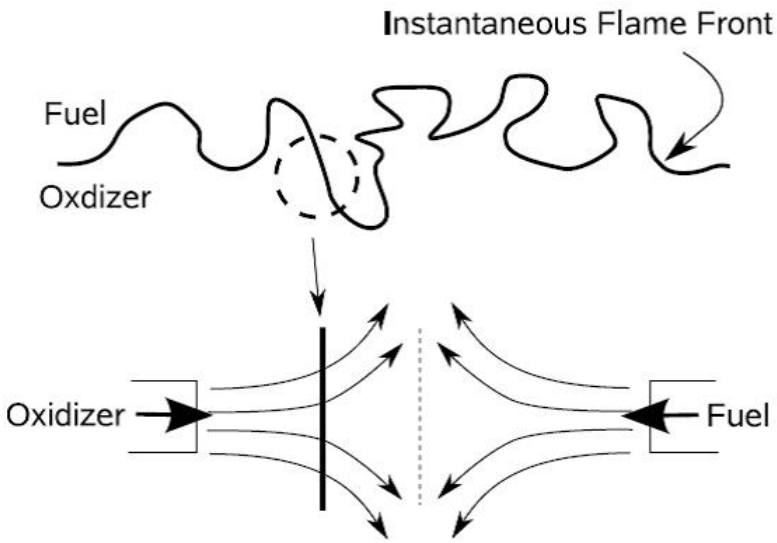

Fig. 2.1. Laminar flamelet concept in a turbulent reacting flow

it is equal to 1 in fuel stream, and regardless of chemical reaction is conserved. This conserved scalar is introduced to account for mixing between the fuel and oxidizer steams. In reaction space with mixture fraction as the coordinate system, energy and species transport equations are solved in 1D mixture fraction coordinate instead solved in 3D physical space. Therefore, inherently this type of combustion modeling is computationally cheaper than methods which do direct integration of chemical reaction in 3D physical domain. However, some techniques such as multi-zone technique has sped up computational time for chemistry calculation in 3D physical space methods.

The laminar flamelet equations can be derived from species and temperature transport equations. A transformation from Cartesian coordinate system to a coordinate system attached to the flame surface is applied. It is assumed that no significant change occur in tangential direction to the flame. So it leads to instead of solving transports equations for species and temperature on 3D Cartesian coordinate (x, y, z) a 1D equation on reaction space with mixture fraction (Z) as coordinate system is solved.

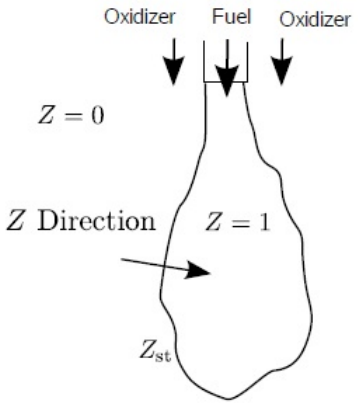

Fig. 2.2. Direction of the largest gradient in reactive species in a non-premixed combustion

Not only this leads to less computation time, but also does it could lead to better prediction on emission as chemistry time is decoupled from CFD calculation; however, for better emission prediction more investigation on accuracy of probability of density functions (PDF) on different combustion conditions and also investigation on heterogeneous effects in CFD field such as spray cooling are still required for RIF model. The laminar flamelet equations by assuming constant Lewis number for all species are given by:

$$\rho\frac{\partial Y_i}{\partial t} - \rho\frac{\chi}{2Le_i}\frac{\partial^2 Y_i}{\partial Z^2} = \dot{\omega}_i \tag{2.7}$$

$$\rho\frac{\partial T}{\partial t} - \rho\frac{\partial^2 T}{\partial Z^2} - \rho\frac{\chi}{2C_p}\Big[\sum_{i=1}^{n}\frac{C_{pi}}{Le_i}\frac{\partial Y_i}{\partial Z} + \frac{\partial C_p}{\partial Z}\Big]\frac{\partial T}{\partial Z} = \frac{1}{C_p}\Big[\frac{\partial P}{\partial t} - \sum_{i=1}^{n}\dot{\omega}_i h_i\Big] \tag{2.8}$$

where ρ is density, T is temperature, C_p is the specific heat capacity, t is the time, Le is Lewis number, $\dot{\omega}$ is net chemical production rate, Y_i is the mass fraction of the chemical species i, h_i is the enthalpy of the chemical species i, n denotes the number of chemical species and χ is the scalar dissipation rate and defined as follow.

$$\chi = 2D(\frac{\partial Z}{\partial x_k})^2 \tag{2.9}$$

By solving this equation at each time step Y as function of Z is obtained. χ or scalar dissipation rate is the most important term in flamelet equation. Scalar dissipation rate contain the information of turbulence and it acts like a bridge between physical space and reaction space. Turbulence is characterized by fluctuating quantities. In RANS modeling of turbulent flow, the mean value of quantities is of interest and fluctuating part is modeled. Mixture fraction like other quantities in turbulent field has mean and fluctuating terms.

$$Z = \tilde{Z} + Z'' \tag{2.10}$$

In turbulent condition, calculating scalar dissipation rate from Eq.2.9 is difficult as it requires the instantaneous value of Z. In addition, the gradient of mean Z on x can be neglected and scalar dissipation rate can modeled as follows:

$$\tilde{\chi} = C_x \frac{\epsilon}{k} \tilde{Z''}^2 \tag{2.11}$$

In this equation scalar dissipation rate, χ , is function of $(t, \overrightarrow{x})$, however, χ should be determined as a function of Z in order to be used in solving the flamelet Eq. 2.7 and Eq. 2.8 . The functional dependency of χ on Z over a known function is given by following equation:

$$\chi(Z) = \chi_{st} \frac{f(Z)}{f(Z_{st})} \tag{2.12}$$

where $f(Z)$ is given by following formula:

$$f(Z) = e^{-2[erfc^(-1)(2Z)]^2} \tag{2.13}$$

A relation between mean χ and mean χ_{st} is given by known PDF function as follow:

$$\tilde{\chi} = \int_0^1 \tilde{\chi}_Z \tilde{P}(Z)\, dZ] = (\tilde{\chi}_{st}) \int_0^1 \frac{f(Z)}{f(Z_{st})} \tilde{P}_z\, dZ \tag{2.14}$$

which lead to evaluate the mean χ_{st} at $(t, \overrightarrow{x})$

$$< \tilde{\chi_{st}}(t, \overrightarrow{x}) >= \tilde{\chi}(t, \overrightarrow{x}) \frac{f(Z_{st})}{\int_0^1 f(Z)\tilde{P(z)}\, dZ} \tag{2.15}$$

Conditional scalar dissipation rate from above formula is calculated at each cell, however, in order to be used in Eq. 2.12, it should be averaged over stoichiometric surface.

Pitsch [27] showed that the surface averaged integral can be evaluated by volumetric averaged integral over domain for conditional scalar dissipation rate at stoichiometric mixture:

$$< \tilde{\chi}_{st} >= \frac{\int_V < \chi_{st} >^{3/2} \overline{\rho}\tilde{P}(Z_{st})\, dV'}{\int_V < \chi_{st} >^{1/2} \overline{\rho}\tilde{P}(Z_{st})\, dV'} \tag{2.16}$$

Once the value of averaged conditional scalar dissipation rate is obtained from above formula it can be used in Eq. 2.12 to calculate scalar dissipation rate which is used in flamelet Eg. 2.7 and Eq. 2.8. One of the shortness of RIF model is that it uses single nominal or conditional averaged scalar dissipation rate for the whole domain.

As mentioned earlier, in RIF modeling is assumed the width of the reaction zone is much smaller than the characteristic length scale of turbulent eddies. Therefore, the structure of laminar flame is maintained and there is no need to determine the turbulent mean reaction source term. Indeed, the role of turbulence is just wrinkling the flame front by turbulent eddies and its effect and information are provided by scalar dissipation rate in flamelet equations.

In some unsteady flamelet concept such as DI engines, before the end of the injection, a portion of the injected fuel is vaporized and combustion (ignition) starts. Therefore, there is variation in amount of mass particle in the physical domain during the combustion. As mentioned earlier, scalar dissipation rate is the only connection tool between physical space and reaction space, i.e. mixture fraction space, in the RIF model. Therefore, this effect should be considered on scalar dissipation rate. In order to capture the effect of this phenomena on combustion, it is suitable to divide

total injected mass to smaller portions and each mass weighted fraction carried with different flamelets. This concept is covered on multiple-flamelet approach [28]. So, it is not surprising that multiple-flamelet RIF model predicts more accurate ignition delay and lift of length in case of DI engines.

In multiple-flamelets model in the CONVERGE CFD code, the first flamelet is initialized at the start of the spray and additional flamelets are initialized in interval of 0.5 crank angles.

2.3 Adaptive Mesh Refinement (AMR)

In transient flows and combustion, sharp gradients such as shear layers, flames, and fuel atomization zones are not spatially localized or temporally constant. Adaptive mesh refinement (AMR) methods provide adequate resolution of temperature and velocity fields only when and where a fine mesh is needed. [25]. The minimum cell size, dx generated with AMR, and the base size dx_{base} are related to each other by the embedding scale as follows:

$$dx = dx_{base} \times 2^{-(b)} \tag{2.17}$$

In this study an embedding scale,b, of 2 is used. The computational mesh generated at the run time during compression, fuel injection and combustion is presented in Figs. 2.3(a),2.3(b) and 2.3(c) respectively, at cross-sections in the meridional mid-plane of the sector volume.

2.4 Soot Model

The Hiroyasu-NSC model is used to model soot in the CFD code. In this model, the soot mass production can be calculated by a single step correlation between the soot mass formation rate $\dot{M}_{sf}$ and soot oxidation rate $\dot{M}_{so}$ according to Hiroyasu and Kodata model [29].

$$\frac{dM_s}{dt} = \dot{M}_{sf} - \dot{M}_{so} \tag{2.18}$$

The Soot mass formation is calculated by:

$$\dot{M_{sf}} = A_{sf} M_{sf} P^{0.5} exp - \frac{E_{sf}}{RT} \tag{2.19}$$

Where A_{sf}=150, M_{sf} is C_2H_2 mass which is calculated from detailed mechanism, P is the pressure in bar, and E_{sf}=12500 cal/mole. In addition, soot oxidation is determined by Nagle and Strickland-Constable model [30]. The net soot oxidation rate is given by:

$$\dot{M}_{so} = \frac{6 M_{wc}}{\rho_s D_s} M_s R_{total} \tag{2.20}$$

Where M_{wc} is the carbone molecular weight (12 g/mole), ρ_s is the soot density (2 g/cm3), $D_s$is the soot diameter ($3 * 10^{-6}$) and $M_s$is the soot mass. Details of the net reaction rate R_{total} is described by Patterson et al. [30].

2.5 NOx Model

The extended Zel'dovich mechanism is implemented in the CFD code to describe the NO formation [31]. This mechanism is given by following reactions:

$$O + N_2 \Longleftrightarrow NO + N \tag{2.21}$$

$$N + O_2 \Longleftrightarrow NO + O \tag{2.22}$$

$$N + OH \Longleftrightarrow NO + H \tag{2.23}$$

An additional factor 1.533 (the ratio of molecular weights of NO_2 to NO) is used to convert the predicted NO to NOx.

2.6 Apparent Heat Release Rate

To better understand the predictions, apparent heat release rate (AHRR) is defined and computed from the experimental pressure data, assuming ideal gas properties for cylinder contents. The AHRR in direct injection engines accordingly is [32]:

$$\frac{dQ_n}{dt} = \frac{\gamma}{(\gamma - 1)} P \frac{d\forall}{dt} + \frac{1}{1+\gamma} \forall \frac{dP}{dt} \tag{2.24}$$

Above, P is pressure, γ is specific heat ratio, C_p/C_v and $\forall$ is instantaneous cylinder volume that it is defined at each crank angle (CA), θ, as follows:

$$\forall = \forall_c[1 + 0.5(r_c - 1)[R + 1 - \cos(\theta) - (R^2 - \sin(\theta - \pi))^2]] \tag{2.25}$$

Above, $\forall_c$ is the clearance volume, r_c is compression ratio and R is ratio of connecting rod length to crank radius [32].

There are more sophisticated models for HRR analysis based on variable gas properties, that also account for the heat transfer and crevice effects. However, the error and accuracy of these models dependent on the accuracy of heat transfer model, crevice effect and mixture non-uniformity [32]. In order to be consistent in both simulation and experimentation, and to keep the focus of the paper on duel-fuel combustion issues, all AHRR are calculated by Eq. 2.24.

2.7 Swirl Number

The swirl ratio is the ratio of the angular spped of the flow, Ω_{flow}, to the angular speed of the crankshaft, $\Omega_{crankshaft}$, with the direction of swirl consistent with the right-hand rule as follows:

$$Swirl_{ratio} = \frac{\Omega_{flow}}{\Omega_{crankshaft}} \tag{2.26}$$

The swirl ratio that is called swirl number in some references cannot lonely represents the velocity profile in the engine accurately since the velocity diminish sig-

nificantly near the cylinder wall. In the code, the Bessel function is used to more accurately represent the velocity profile in the engine [33].

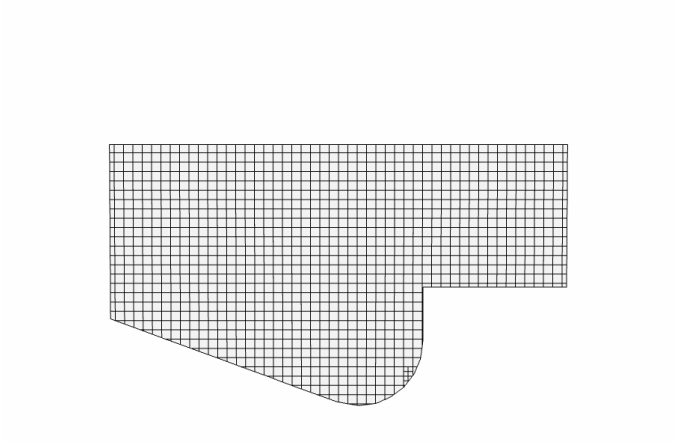

(a) -32 CA (compression).

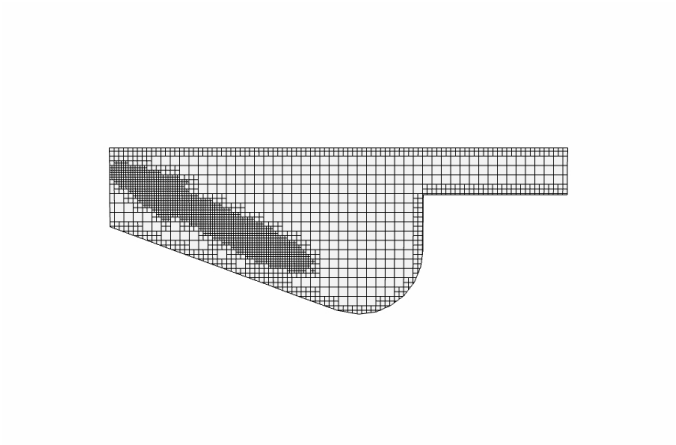

(b) -12 CA (fuel injection).

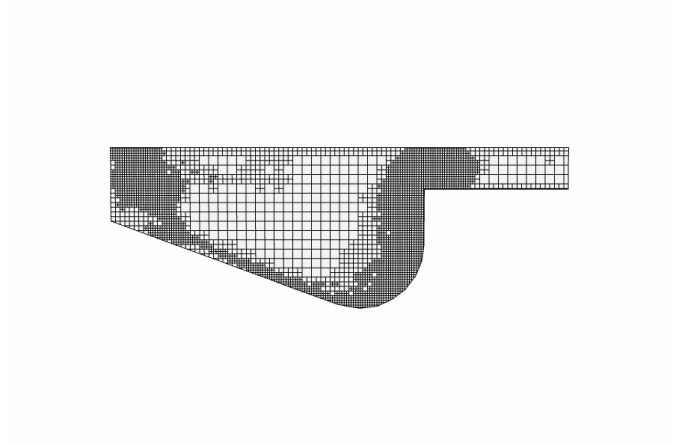

(c) 11 CA (combustion).

Fig. 2.3. Computational mesh with adaptive variation versus crank angle(CA)

3. INITIAL AND BOUNDARY CONDITIONS

As it can be seen from Fig. 3.1, the geometry has 5 walls. It is a close system with no mass exchange from the system's boundaries. The thermal conditions of the walls are also shown in the Fig. 3.1 and the suggested values are extracted from reference [34]. It is assumed that the temperature is constant and the walls follow the" law of wall" with 0 roughness.

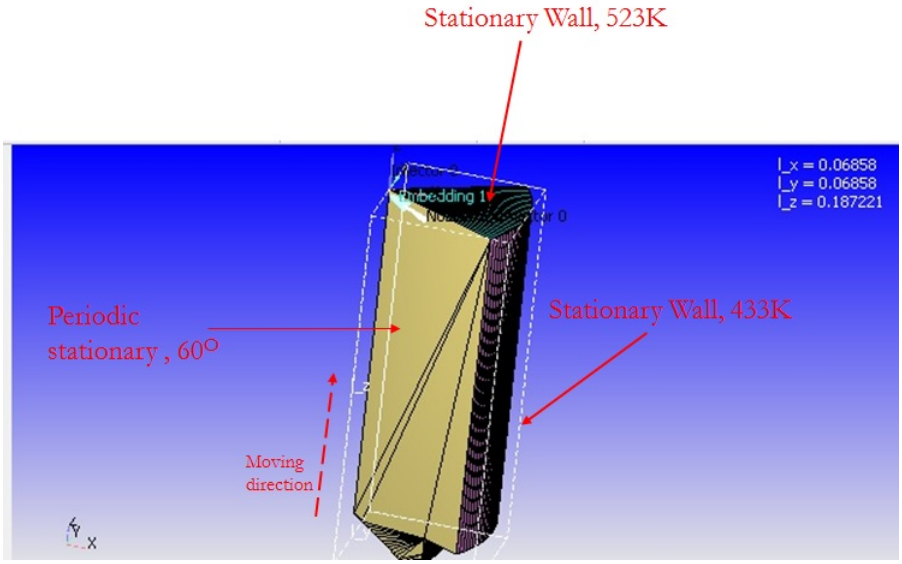

Fig. 3.1. Boundary conditions of the case

The initial velocity is characterised by swirl number and swirl profile. The turbulence is initialized by the turbulence kinetic energy and turbulence dissipation in the RNG k-ϵ framework. The suggested value for the above parameters are summarized in Table 3.1. The initial species at the start of the simulation are CH_4,N_2 and O_2, and later around top dead dead center (TDC) liquid C_7H_{16} is injected directly in the cylinder.

Table 3.1.
Summary of initial conditions in the NGD dual-fuel engine

Swirl number	0.978
Swirl profile	3.11
Turbulence kinetic energy (m2/s2)	62.027
Turbulence dissipation (m2/s3)	17183.4
Start of simulation	-147 CA

4. SIMULATIONS OF SINGLE-INJECTION OPERATION

4.1 Grid Convergence Study

Accuracy of diesel engine combustion simulation using RANS requires adequate mesh resolution, which has been argued as more important than modeling of sub-grid effects. [25, 27]. The effect of base mesh size on major outcomes of the simulation was examined in this study. Table 4.1 provides details of base mesh size in millimeter(mm), minimum cell size in mm, maximum number of allowed cell and computation time information on 64 processors.

Table 4.1.
Cases considered for grid refinement study

Base mesh size (mm)	**Min cell size (mm)**	**Maximum cell counts (10^6)**	**Simulation time (hrs)**
2	0.5	1	2.47
1.4	0.35	1	6.25
0.8	0.2	1.5	20.88
0.5	0.125	2	70.40

It appears in Fig. 4.1 that the pressure traces and HRR do not change significantly when minimum cell size decreases from 0.2 mm to 0.125 mm. There is a significant difference between the solutions for 0.35 mm and 0.75 mm minimum cell size. Henceforth, the minimum mesh size of 0.2 mm is used for rest of this study.

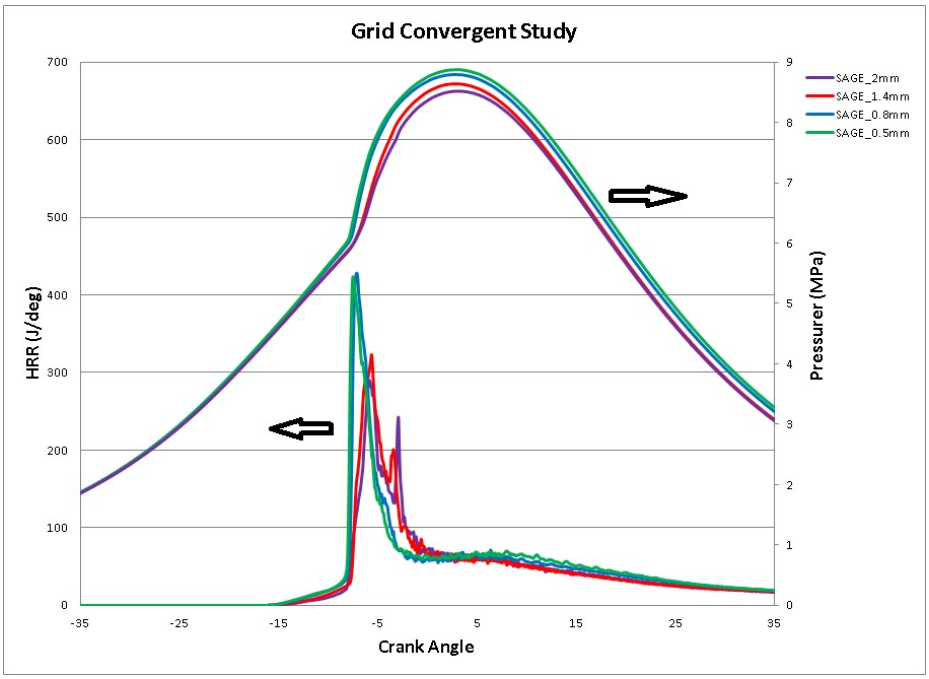

Fig. 4.1. Grid convergence study with a RANS turbulence model for the baseline conditions shown in Table-4.1

4.1.1 The Effect of Processor Numbers on Computation Time

In Fig. 4.2 the effect of number of processors on computational time in multi-processor is shown. In the case of engine sector with the total maximum allowance cell counts of one million and detailed chemistry and AMR, it seems that 64 cores is the optimum number of cores to have minimum computation time. The reason why computation time increases when the number of processors increase is some cores are almost inactive and they do not contribute in computation in load balancing. It can be seen that some ranks got zero value or very small number when the number of processors go beyond a certain number; indeed, the rank indicates the cell numbers are assigned for a certain core in domain decomposing. Therefore, an small number or zero in each rank shows that the core is almost have no contribution in computation and not only they reduce the processing time but also do message passing with the master processor increases the processing time.

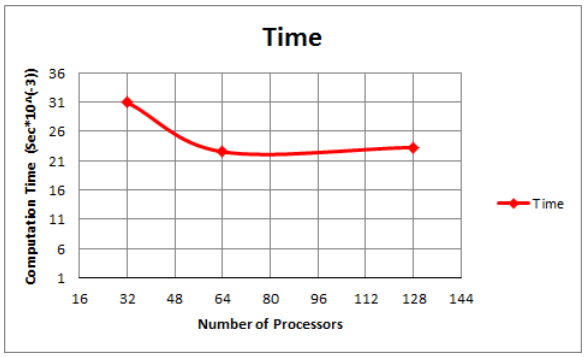

Fig. 4.2. Grid convergence study with a RANS turbulence model for the baseline conditions shown in Table 4.1

4.2 Pressure Trace and Heat Release Rate

The results presented here corresponds to the operating conditions mentioned in Table 4.2. The results from the simulation with chemical reaction mechanism consist of 79-species and 464-reaction mechanism are compared with the experimental results from Singh et al. [35].

The trace of the cylinder pressure appears to capture the timing of ignition and combustion well in 50% and 75% natural gas substitution cases mentioned in Table 4.2, but the magnitude is slightly under-predicted compared to experiment (Fig. 4.3). It should be mentioned that the percent substitution is calculated based on the energy contribution of the fuels, not by the mass contribution.

It seems that the model fails to predict the pressure trace and HRR well, in case of 90% natural gas substitution. Singh et al. [35] states that the model improvement to account for flame-wall interaction could improve the accuracy of the simulation in cases with more than 90% natural gas substitution. In addition, many experimental studies show high level of cycle to cycle variation (CCV) in pressure traces and weak atomization in diesel injection for more than 90% natural gas substitution [36]. Therefore, this study is limited to cases that the equivalence ratio of premixed mixture of natural gas and air is less than 0.3 or; in the other words, the level of natural gas substitution is less than 85%.

Table 4.2.
Operating conditions of CAT-3401 diesel engine under natural gas-diesel dual-fuel mode

	50% of total energy from natural gas	75% of total energy from natural gas	90% of total energy from natural gas
Engine speed (rpm)	1960	1960	1960
Total mass of injected NG (g/cycle)	0.0419	0.0712	0.0917
Total mass of injected diesel (g/cycle)	0.0487	0.0270	0.0117
Start of injection (CA)	-22	-22	-22
Injection duration (CA)	-14.5	9.5	6.5
Inlet temperature at start of compression (°C)	75	75	75
Premixed charge equivalence ratio	0.15	0.27	0.35

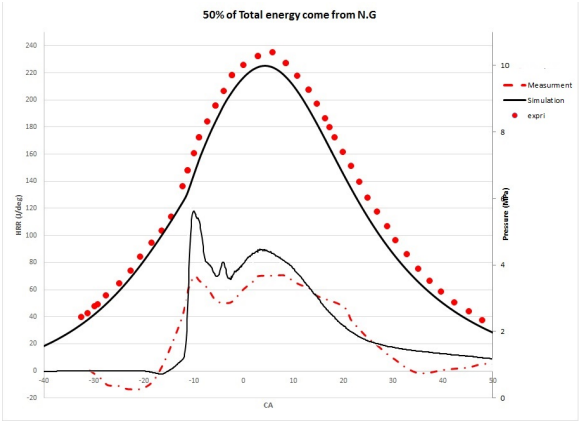

(a) 50% of total energy comes from NG

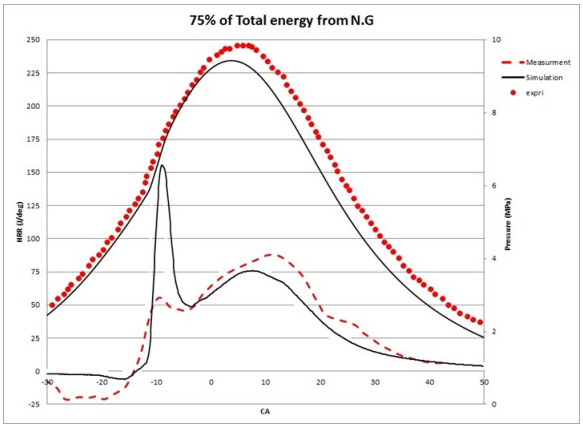

(b) 75% of total energy comes from NG

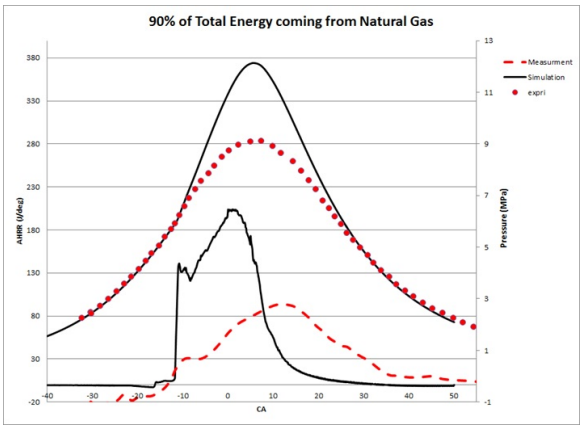

(c) 90% of total energy comes from NG

Fig. 4.3. Comparison of in-cylinder pressure and HRR prediction from RANS simulation and averaged pressure trace and measured HRR from experiment data.

For 50% and 75% natural gas substitution, the experimental AHRR profile is reasonably well modeled, but with a sharper initial spike and less prominent endothermic period of fuel evaporation. The initial AHRR spike is associated with premixed combustion of the injected fuel, which depends on the mass of air is enveloped by the evaporating fuel. The predicted AHRR also indicates longer overall combustion duration in comparison with measured AHRR. Other researchers have reported similar behavior for pressure and AHRR in NGD dual-fuel engine in the same range of equivalence ratio for different engines. Issues related to HRR calculation from experiment and simulation are well discussed in References [26, 28, 29].

4.3 The Role of Chemical Reaction Mechanism

The chemical reaction mechanism which is used in this study has 76-species and 464-reaction mechanism, for instance, the results shown in Fig. 4.3 have used this mechanism for chemical kinetic calculation. The number of species and reaction mechanism plays an important role in 3D reactive flow cases that computational time is the major concern. Another chemical reaction mechanism, which consists of 29-species and 54-reaction mechanism and suggested by other researches [2] in simulation of NGD dual-fuel engine is implemented in the case setup and its predicted pressure and HRR are compared with the last case [1].

One of the important roles of chemical reaction mechanisms in IC engine simulation is accurate predication of ignition delay. As shown in Fig. 4.4, the large mechanism (a 76-species 464-reactions mechanism) predicts the ignition delay reasonably accurate in NGD dual-fuel engine.

In Fig. 4.4, the results of pressure traces and HRR are compared for both mechanisms to reveal the role of reaction mechanism on combustion of NGD dual-fuel engine. It can be seen that the small mechanism (a 29-species and 54-reaction mechanism) predicts a longer ignition delay which is not the main interest in this study

[1]The chemical reaction mechanism consist of 29-species and 54-reactions are fully described in Appendix.B

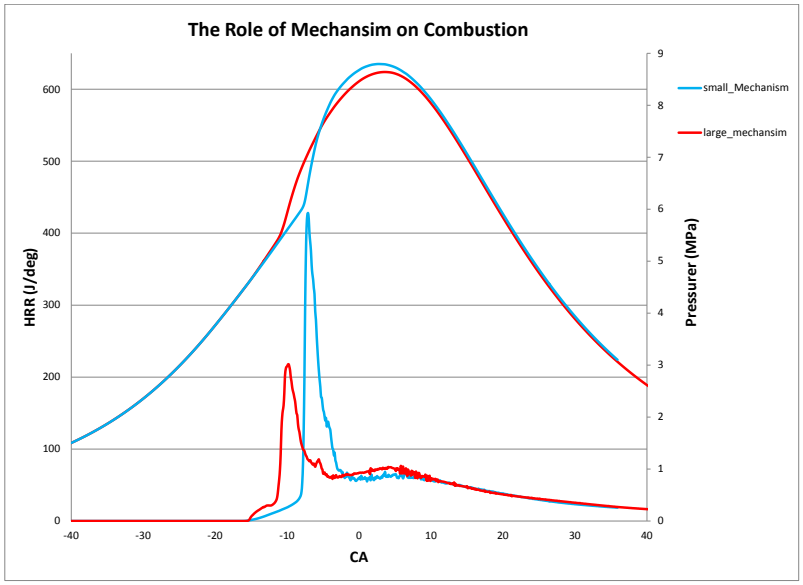

Fig. 4.4. The role of chemical mechanism on pressure and HRR prediction in NGD dual-fuel engine

at least. In addition, it can be concluded that the simulation with small mechanism predicts ignition even in larger volume than the simulation with large mechanism. Therefore, for rest of the paper the results presented are based on simulations with the large mechanism. However, it should be noted that the computational time when a larger mechanism is used increase by 119%.

4.4 Combustion Mode in NGD Dual-Fuel Engines

Among the significant questions regarding NGD dual-fuel engines is whether combustion is dominated by auto-ignition, flame propagation, diffusion or a combination of these combustion modes. It is also of interest to know the effect of combustion and control parameters on engine performance. These issues can guide development, bet-

ter control and more precise optimization of dual-fuel engines, and to develop more reliable computational models.

For deeper understanding of the methane combustion regime, it is useful to examine local equivalence ratio throughout the chamber. In the CFD code, equivalence ratio is defined in each computational cell as follows:

$$\Phi = \frac{2\sum_i N_i \eta_{c,i} + 1/2 \sum_i N_i \eta_{H,i}}{\sum_i N_i \eta_{O,i}} \tag{4.1}$$

Where N_i is the number of moles of species i and $\eta_{C,i}$ $\eta_{H,i}$ and $\eta_{O,i}$ are the number of Carbon (C), hydrogen (H) and oxygen (O) atoms, respectively, for species i. This definition does not differentiate based on the source of each atom, and should be interpreted carefully if there is residual exhaust gas (not considered in the present work).

A sequence of images is presented in Fig. 4.5 that shows the temperature level plots in the mid-plane of the modeled 60-degree cylinder sector, together with the three-dimensional distribution of liquid fuel parcels. It is meaningful to consider combustion to occur in multiple stages. The first stage extends along the injection trajectory, with injected fuel evaporation to form a premixed-mixture that ignites as a mass. The second stage involves the liquid droplets that reach the piston bowl wall, with evaporation in the arch region of the piston bowl [30].

As seen in Fig. 4.5(d), there is some amount of liquid that exist even after 30 degrees CA. The amount of unburned liquid diesel at 30 CA is 0.191 milligram (mg) which is equal to 2.4% of the total injected diesel fuel. But the size of these liquid fuel parcels are magnified for better visualization in Fig. 4.5(d). The motion of these parcels is also toward the low temperature regions as shown in the figure; These liquid parcels moving into unburned premixed regions can ignite later and help complete combustion, or may reach too late in the expansion process. This phenomenon can have an implications for unburned hydrocarbon emissions in an operating NGD dual-fuel engine.

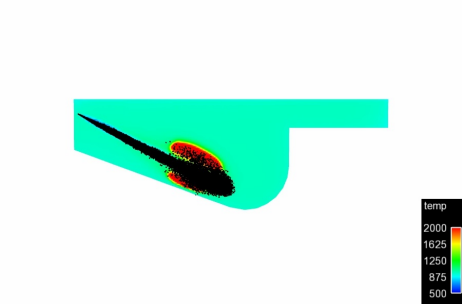

(a) temperature level in the mid-plane at -10CA

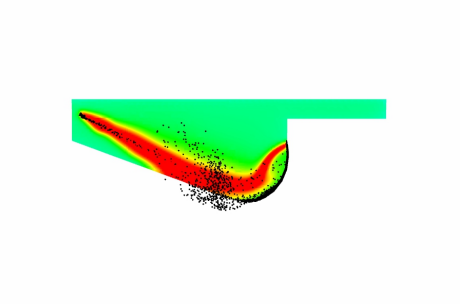

(b) temperature level in the mid-plane at -1CA

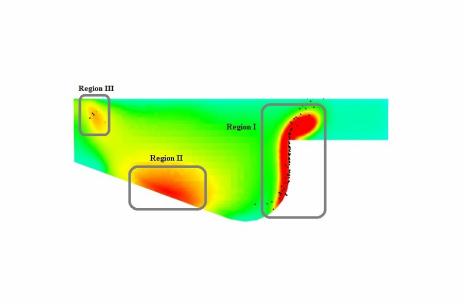

(c) temperature level in the mid-plane at 17CA

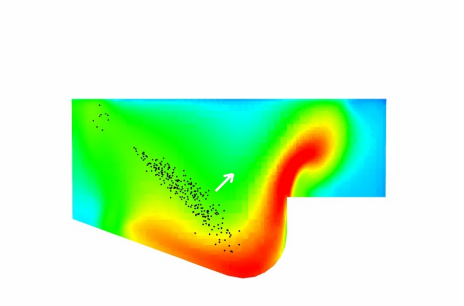

(d) temperature level in the mid-plane at 33CA

Fig. 4.5. Temperature profile in the mid-plane of the modeled 60-degree cylinder sector with liquid fuel parcels distribution(All figures are at same temperature spectrum as part-a)

Fig. 4.6 shows the variation of CH_4 and C_7H_{16} total mass versus crank angle time. The black and green curves show liquid and vapor form of C_7H_{16}, respectively, and blue curve shows the accumulated mass of C_7H_{16}, which is equal to the total amount of injected diesel (48.7 mg) at the end of the injection duration. It can be seen that after 50 CA, almost all of the C_7H_{16} burned and around half ofCH_4 is still unburned. It reveals that main part of unburned hydrocarbons (HC) emission in NGD dual-fuel engines are corresponded to unburned CH_4.However,to understand in more detail how diesel and gas fuels are consumed and how we can burn the CH_4 more efficiently. Besides, to figure out the nature of the combustion regime (i.e. flame propagation, auto-ignition, or diffusion) at each stage it is instructive to examine methane and n-heptane distribution and equivalence ratio history in the cylinder. The two vapor-phase fuel distributions in the mid-plane of the engine sector are shown in Fig. 4.7.

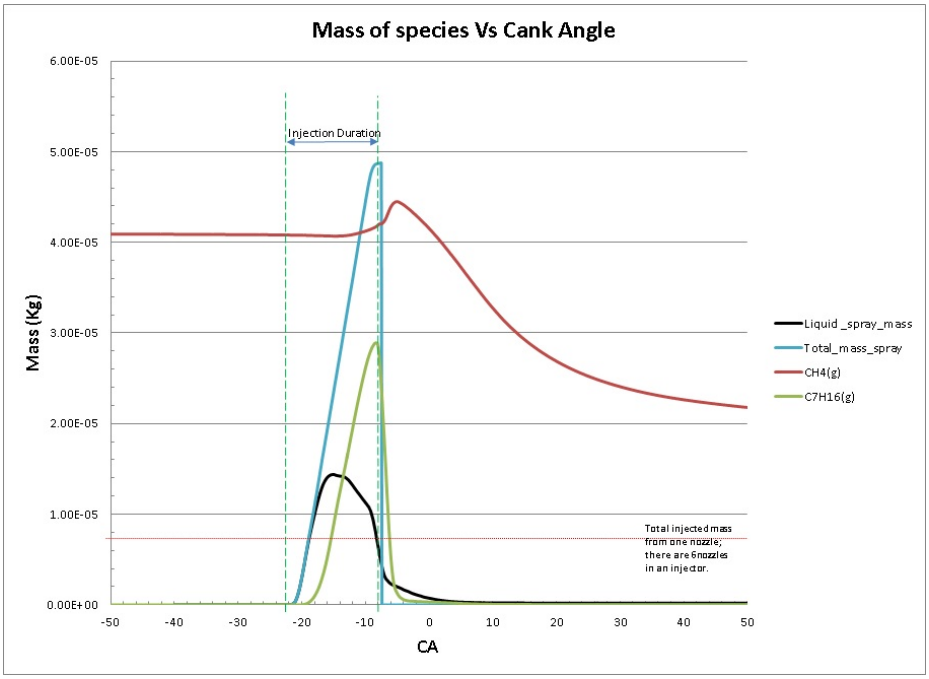

Fig. 4.6. Variation of methane and liquid and gas phase of n-heptane versus crank angle time

As expected, the combustion starts with combustion of vaporized diesel fuel in an annular region around the line of injection, and is accompanied by the combustion

of methane in same region. By 17 CA, the last remnant of n-heptane near the bowl region is consumed, except for late evaporating droplets seen in Fig. 4.5. On the other hand, it is seen from Figs. 4.7(e) and 4.7(g) that significant methane remind unburned mainly adjacent to the cylinder wall and near the cylinder head, which would lead to unburned hydrocarbons in such fuel-lean NGD dual-fuel engines.

In Fig. 4.5(c), three distinct high temperature regions can be observed at 17 CA when essentially all n-heptane vapor has been consumed. It appears that in "Region I" combustion starts with auto-ignition of a small amount of n-heptane vapor and then through a mixing controlled process between hot products and fresh mixture progress. By comparing the Figs. 4.7(e) and4.7(g) with Figs. 4.5(c)-4.5(d) seems like flame propagation in premixed mixture might have happened in "region II" and "region III". Examining the equivalence ratio distribution in Fig.4.9. It shows that in regions II and III, equivalence ratio is around 0.5 at 17 CA and 33 CA (Fig. 4.9(c) and Fig. 4.9(d)).

Singh et al. [20] used PREMIX code [37] to predict laminar flame speed in conditions similar to IC engine. They showed that flammability limit for natural gas-air mixture in conditions similar to IC engine could be as low as 0.3 (Fig. 4.8). Therefore, it is not surprising if flame propagation behavior is observed in "regions II and III". Even though flame propagation would happen in "regions II and III", it seems flame can not develop in regions near to the walls as equivalence ratio of the mixture is too low in those regions that flame cannot develop there. In addition, as immediate environment near "regions II and III" are occupied by low equivalence ratio regions, the portion of combustion associated with flame propagation is not large part of heat release and combustion in case of 50% natural gas substitution.

Fig. 4.9(a) shows that by injecting the diesel fuel in the premixed mixture of natural gas and air, the premixed mixture turn to heterogeneous mixture. The fuel injection increases the level of turbulence in cylinder and in same time creates a stratified mixture which is richer near position bowl and leaner in the middle and top of the cylinder. This mixture stratification is the main challenge for this type of

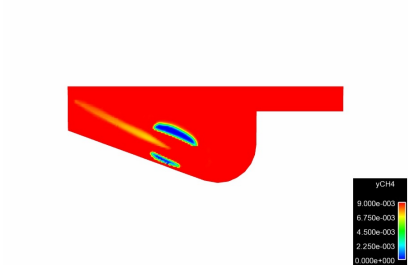

(a) Methane mass fraction distrbution at -10CA

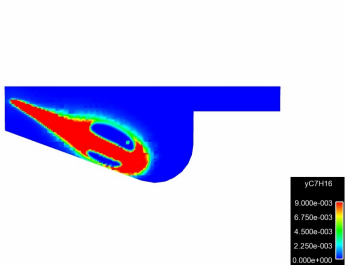

(b) n-Hepthane mass fraction distrbution at -10CA

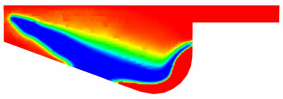

(c) Methane mass fraction distrbution at 1CA

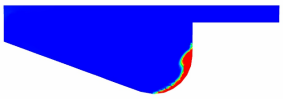

(d) n-Hepthane mass fraction distrbution at 1CA

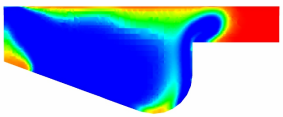

(e) Methane mass fraction distrbution at 17CA

(f) n-Hepthane mass fraction distrbution at 17CA

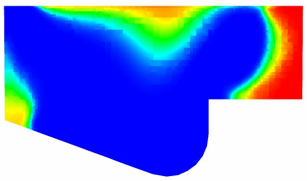

(g) Methane mass fraction distrbution at 33CA

Fig. 4.7. Vapor phase distribution of methane and n-hepthane at mid-plane of engine sector.

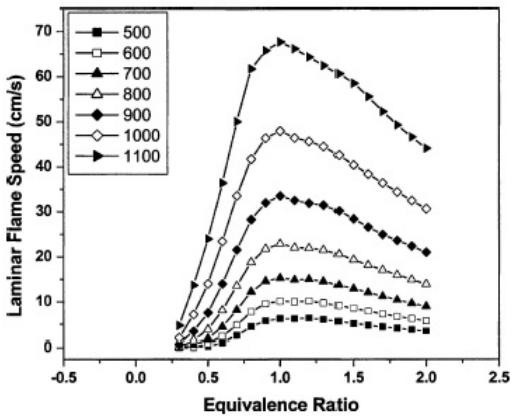

Fig. 4.8. Laminar flame speed for mixture of methane and air at 8MPa as a function of equivalence ratio and unburned gas temperature calculated by the PREMIX code [37].

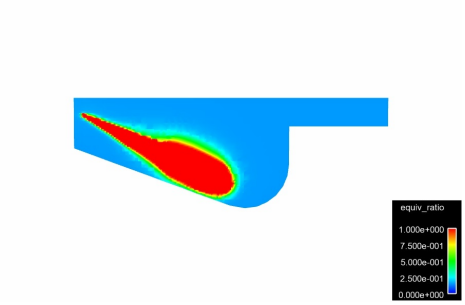

(a) Equivalence ratio distribution at -10CA

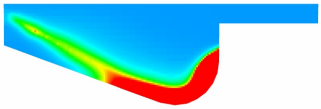

(b) Equivalence ratio distribution at -1CA

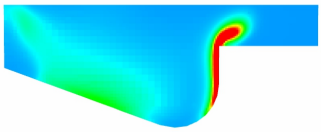

(c) Equivalence ratio distribution at 17CA

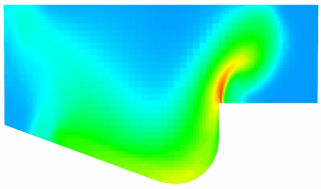

(d) Equivalence ratio distribution at 33CA

Fig. 4.9. Equivalence ratio distribution in mid-plane of engine sector.

charge in NGD dual-fuel engines, so many researchers have investigated the different strategies such as multiple injection or direct injection of natural gas for NGD dual-fuel engines [4, 31].

Dronniou et al. [38] investigated combustion in an optically accessible light-duty NGD dual-fuel engine at low and high equivalence ratio, with port injection of natural gas and direct injection of diesel fuel. The size and geometry of the tested engine is different from the engine modeled in the present work. Their OH chemiluminesence images are presented in Fig. 4.10 for low equivalence ratio ($\phi < 0.6$) of the gas-air mixture.

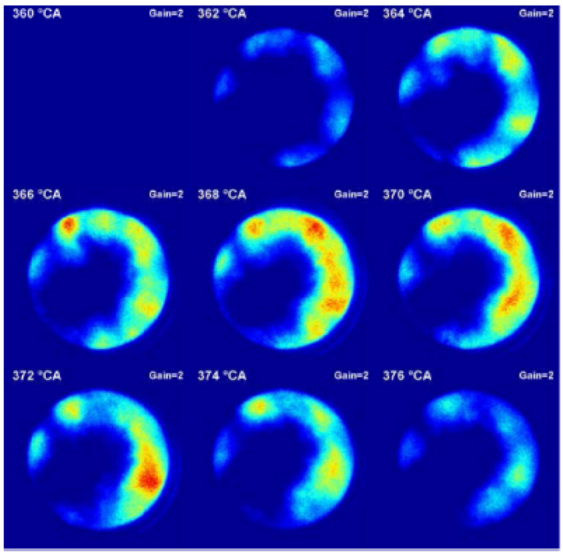

Fig. 4.10. OH chemiluminescence images for the $\phi_{premixed} = 0.5$ condition [38]

Dronniou et al. [38] reported that gas-air mixtures with high equivalence ratio ($\phi >$ 0.8) exhibit combustion that is dominated by flame propagation in their experiment [30]. Such operation may be expected in an engine purposely designed for dual-fuel operation with anticipation of all of the thermal, pressure, and structural implications of such a design. However, the equivalence ratio at which combustion of NGD dual-fuel engine begins to exhibit flame propagation behavior as dominate combustion

mode is not well defined, given that the limited research used different engines and conditions [16, 30].

Conversely, it can be expected that NGD dual-fuel combustion in relatively leaner mixtures ($\phi < 0.6$) would be dominated by diffusion combustion. This would be typically expected if an engine originally designed as a diesel engine is converted to dual-fuel operation within the same range of rated load.

For conditions in NGD dual-fuel engine with diffusive combustion as the dominate combustion mode, it may be worthwhile to consider combustion models for non-premixed (diffusion) combustion such as the representative interactive flamelet (RIF) model to see whether mixing controlled combustion is the dominate combustion mode or not. In addition, one advantage of RIF model in comparison with SAGE model (detail chemistry without turbulence chemistry interaction) is that it considers turbulence-chemistry interaction. A single-flamelet RIF model may be significantly less expensive in computation, as it solves the chemistry in 1D reaction zone coordinate instead of 3D chemistry calculation with SAGE solver [2].

In Fig. 4.11 the results for the pressure trace and the HRR from RIF model is compared with SAGE combustion model (no turbulence-chemistry interaction model). As can be seen from the figure the results for pressure is really close in both models and it reveals that combustion is mainly dominated by diffusion. A sharp peak can be observed in the premixed burn spike from RIF model. This shows that single flamelet RIF model predicts larger volume in premixed burn spike than SAGE model. this issue might have been addressed by multiple flamelet RIF model, but as it is not the main scope of this work is not considered here. In addition, it is helpful to mention that the HRR results from the simulations needed to be filtered and these results just show the raw, unfiltered HRR, more discussion in this regard can be found in ref [28].

Fig. 4.12 compares the temperature level at mid-plane of the engine sector by both SAGE and RIF model. It shows that RIF model predicts ignition in larger

[2] The computational time in RIF model increase with increase of the number of flamelet- a single flamelet that is parameterized by a representative scalar dissipation across the entire combustion chamber is used here.

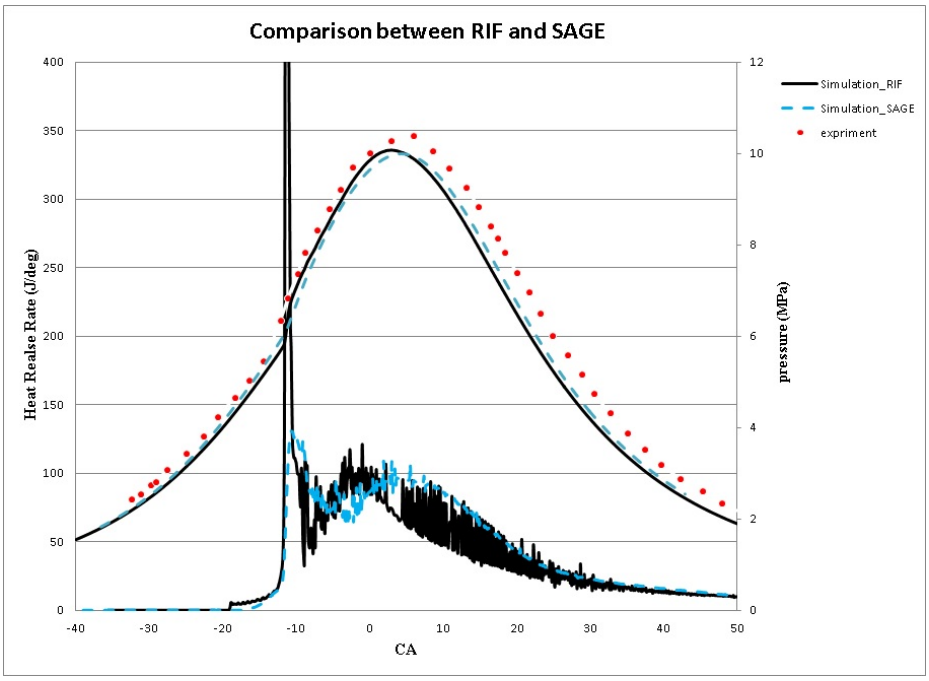

Fig. 4.11. Comparison between RIF and SAGE combustion model in NGD dual-fuel engine in case of 50% natural gas substitution.

volume as it can be seem from Fig. 4.12(a). In addition, it seems that in contrast to the SAGE model, the RIF model does not predict combustion in regions II and III and it predicts combustion in larger volume in "region I".

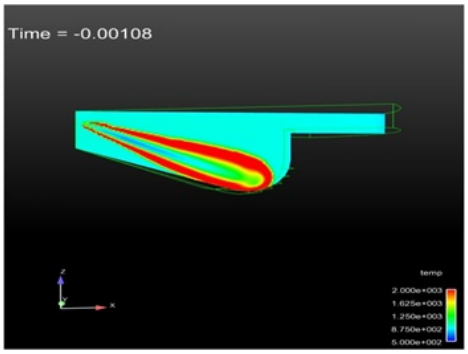

(a) Temperature profile with RIF combustion model at -10CA

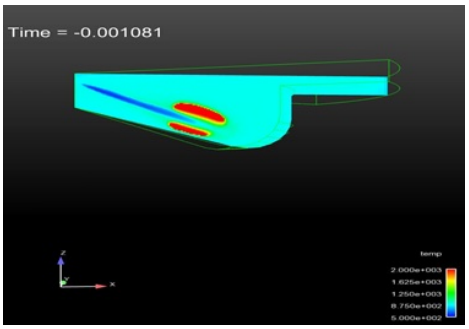

(b) Temperature profile with SAGE combustion model at -10CA

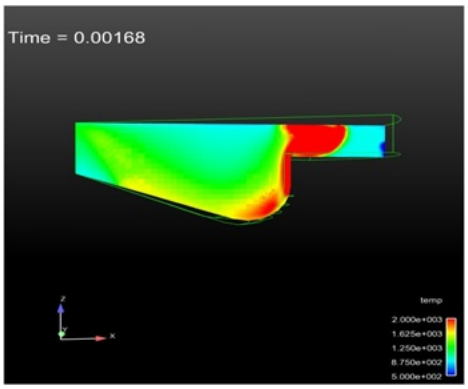

(c) Temperature profile with RIF combustion model at 17CA

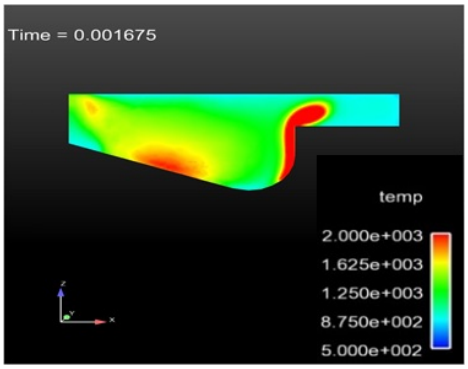

(d) Temperature profile with SAGE combustion model at 17CA

Fig. 4.12. Comparison of temperature level between RIF and SAGE combustion model in NGD dual-fuel engine.

5. SIMULATION OF MULTI-INJECTION OPERATION

As mentioned in the last chapter, the main challenge of NGD dual-fuel engine is high level of unburned hydrocarbon emission (HC emission). The details of flow motion provided by the CFD results reveal that due to the low equivalence ratio of the premixed mixture, flame cannot develop in the regions adjacent to the walls, and the main part of unburned hydrocarbon is associated with unburned CH_4. Therefore, any idea that allows injected high-reactive fuel to mix with more low-reactive fuel could decrease the HC emission. In addition, small portion of HC emission is from the unburned liquid parcels of diesel fuel at the end of combustion.

According to the above observations from CFD results, some parameters are selected and their effects on pollutants are considered. In this chapter, NO_X, Soot and HC emissions are modeled based on the modeling approaches summarized in Table 5.1 to quantitatively consider the effect of selected parameters on emissions.

Table 5.1.
Emission models applied for the NGD dual-fuel engine

	NOX emission	**Soot emission**	**Hydrocabone emission**
Model	Extended Zeldovich	Hiroyasu-NSC	76-species 464-reactions mechanism

The results of emission in heavy-duty CAT-3401 engine at 21 kW (40% load) and 1690 rpm for 0% natural gas substitution (i.e. conventional diesel engine mode) and 50% natural gas substitution are shown in Table 5.2. It can be seen from both experiment and simulation results that HC emission increases as result of more natural gas substitution(Table 5.2). Same trend is observed by other researchers as results of natural gas substitution in NGD dual-fuel engines [39, 40]. In addition, the results of HC emissions with and without a model for crevice flow show a significant difference.

It can be concluded that more precise model for the crevice flow is required in NGD dual-fuel engines. However, the trend of the results is enlightening enough to go further and investigate the effect of the different parameters on the engine performance based on the CFD simulation results.

Table 5.2.
Emission results in CAT-3401 diesel engine in the part-load condition

	HC (g/kwh)			NOX (g/kwh)		Soot (g/kwh)	
	Experiment	Simulation with crevice flow model	simulation Without crevice flow model	Experiment	Simulation	Experiment	Simulation
0% Natural gas substitution	0.21	0.37	N/A	13.9	7.38	N/A	2.55
50% Natural gas substitution	25	53.6	9.8	5.5	5.82	N/A	1.57

5.1 Numerical Investigation of NGD Dual-Fuel Engine for the Purpose of Hydrocarbon Emissions Reduction

As mentioned earlier the main challenge of NGD dual-fuel engines besides many promising features is high level of HC missions. The CH_4 and C_7H_{16} mass fraction variation versus time is shown in Fig. 5.1. The figure shows that the main part of HC emission corresponded to methane while some amount of C_7H_{16} remains unburned, too.

In following the effect of some parameters on combustion and emission of NGD dual-fuel engine for the purpose of HC reduction is considered.

5.1.1 The Effect of Swirl Number on Combustion and Emission

The degree of swirl in the flow can be quantified by dimensionless parameter, Sn, known as the swirl number which is defined as the ratio of the axial flux of angular momentum to the axial flux of axial momentum.

Swirl can improve the turbulence in IC engine and has important effect in spark ignition engines. In this section the effect of the swirl number on combustion and

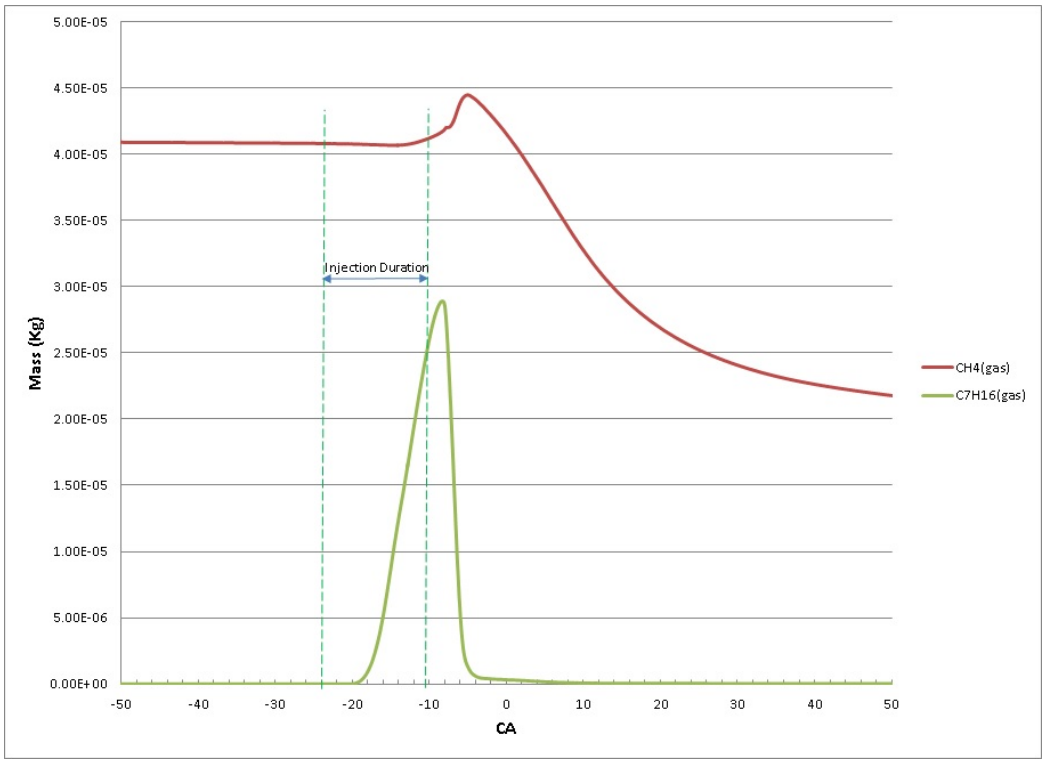

Fig. 5.1. The vapor phase variation of CH_4 and C_7H_{16} versus crank angle (CA) time.

emission in the NGD dual-fuel operation is considered. It should be noted that changing the swirl number in a real engine is required re-designing the inlet charge manifold. Fig. 5.2 shows the effect of swirl number on combustion: the case with low swirl number corresponded to swirl number of 1 and the high swirl number corresponded to swirl number of 2.5. The results reveal that increasing the swirl in engine shortens the ignition delay and it makes the combustion faster. In addition, the swirl has marginal effect on emission. The NO_X and HC emissions do not change significantly by changing the swirl number.

5.1.2 The Effect of Initial Temperature on Emission

The CFD results of temperature profiles show that some of the liquid parcels did not have a chance to vaporize and burn and it can contribute on HC emission.

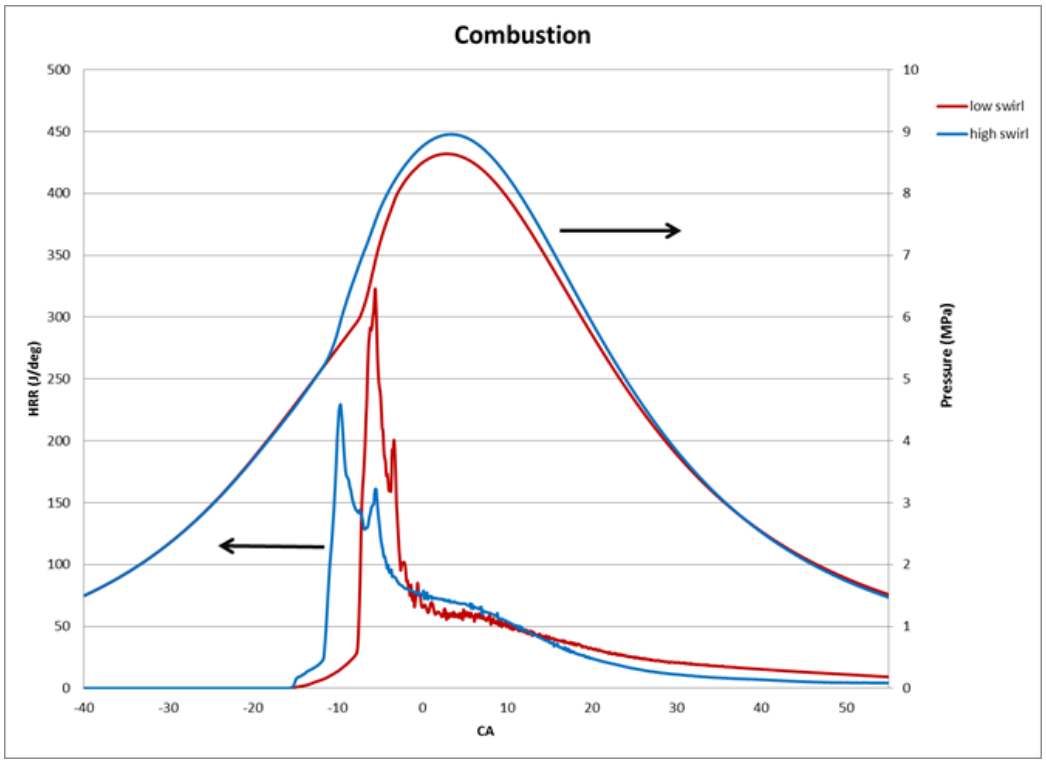

Fig. 5.2. The effect of the swirl number on combustion in NGD dual-fuel engine.

Increasing the premixed mixture temperature at intake port could increase the chance of vaporization of the liquid fuel parcels and consequently decrease the HC emission. Fig. 5.3 shows the effect of increasing initial temperature on HC and NO_X emission. It reveals that increasing the initial temperature could decrease HC emission on part-load NGD dual-fuel engine while slightly increases NO_X emission.

Although by increasing the temperature the NO_X emission increase, the NO_X emission in NGD dual-fuel operation is still less than the same engine when it works under the conventional diesel mode at the same load and rpm. In addition, as the main part of HC emission related to unburned natural gas which sticks near the piston walls and flame cannot reach those regions, increasing temperature does not have a significant effect on HC-emission reduction.

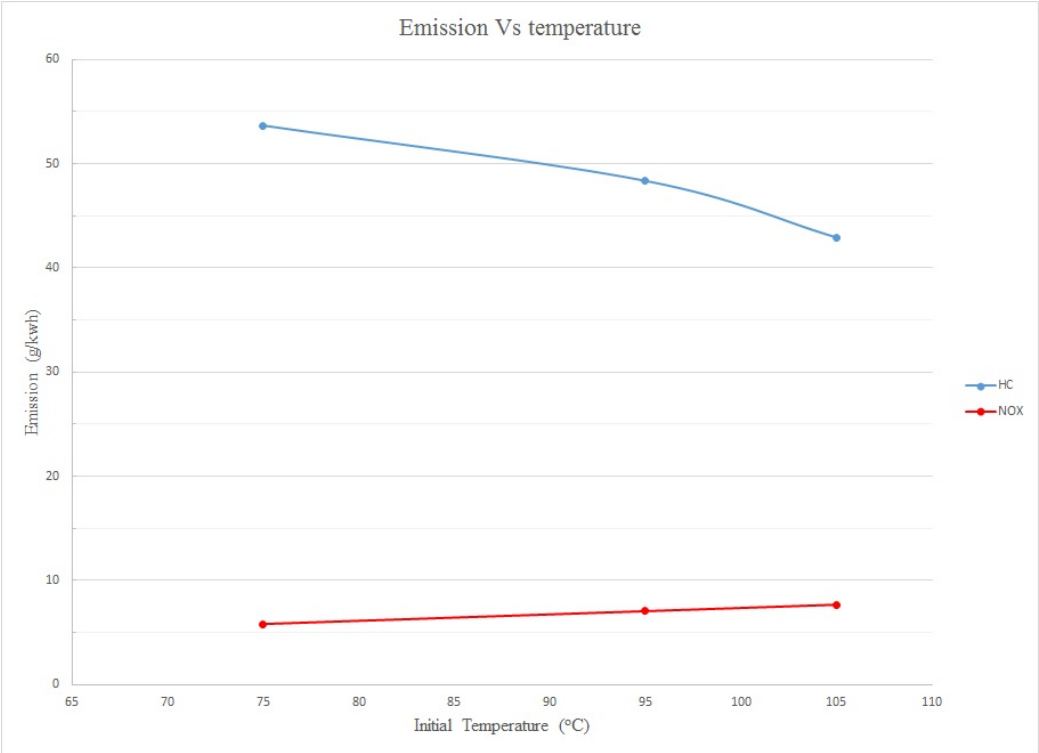

Fig. 5.3. The effect of the initial temperature on NGD dual-fuel engine emission.

5.1.3 The Effect of Initial Pressure on Emission

Diesel engines usually operate with turbocharging and extra air. In NGD dual-fuel engine which operate on a diesel engine, a port fuel injection of natural gas would add to the inlet air manifold of the diesel engine to operate on dual-fuel mode. The amount of natural gas substitution for dual-fuel operation is defined based on energy content as follows:

$$substitution\% = \frac{m_{NG}Q_{NG}}{m_{NG}Q_{NG} + m_dQ_d} \tag{5.1}$$

The equivalence ratio of the premixed mixture at start of compression is between 0.10 and 0.30 when substitution percent is between $40\%-80\%$. Therefore, the mixture of natural gas and air is so lean at start of compression even in cases like 80% natural gas substitution. This equivalence ratio rang is so low that flame cannot propagate on regions that there is no diesel fuel parcels. There are two approaches to make

the mixture richer: one increase the fuel amount, other decrease the air amount. Decreasing air amount could be achieved by decreasing the boost pressure (i.e. initial pressure).

The results presented on Fig. 5.4 shows that HC emission decrease by decreasing boost pressure. The mixture of air and natural gas gets richer and the equivalence ratio of the premixed mixture increases. So, the chance of combustion and flame propagation in natural gas increases. This reduction in the boost pressure could achieved by naturally aspired induction or by bypass in multi-stage turbochargers.

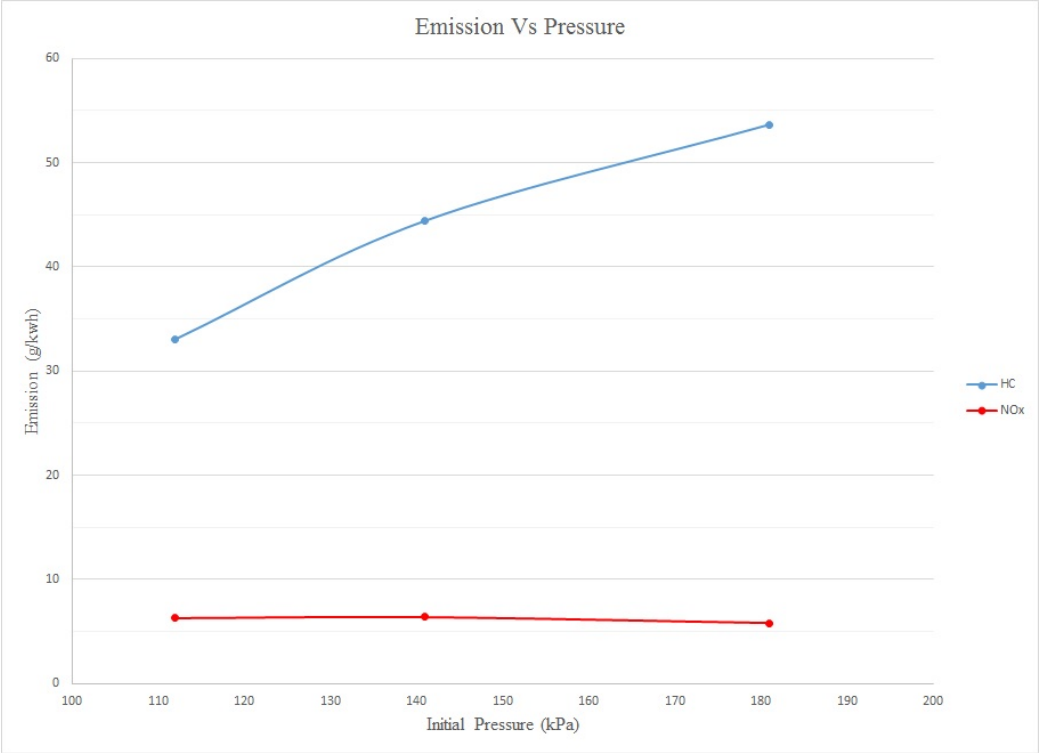

Fig. 5.4. The effect of the boost pressure on NGD dual-fuel engine emission.

5.1.4 The Effect of Multi-injection on Combustion and Emission

As mentioned before, the main portion of HC emissions corresponds to unburned natural gas near the cylinder walls. Direct injection of natural gas could make a

stratified combustion at the middle of the cylinder; plus, multi injection of diesel fuel with one early injection could make a more reactive homogeneous mixture that increase the change of ignition in low reactive methane mixture [1].

There are different strategies for multi-injection of diesel fuel. In this work, multi-injection is limited to double injection of diesel fuel as it expected that the effect could be similar for more than two injections. However, how the fuel amount in each injection should be distributed in each injection is another concern in double-injection strategy that in following is tired to be addressed.

Two different double injection strategies are considered to examine the effect of diesel fuel distribution between the first and the second injection. In the first trial, the main injection is the second injection and close to the top dead center (TDC). While in the second trial, the main injection is the first injection near the bottom dead center (BDC). The details of each case is shown in Table 5.3.

Table 5.3.
Two different double-injection strategies

	First Injection		**Second injection**	
	Amount (mg)	Start(CA)	Amount (mg)	Start (CA)
Trial I	2.44	-80	5.69	-15
Trial II	5.69	-80	2.44	-15

The results of pressure trace and HRR for the cases in Table 5.3 are shown in Fig. 5.5. It can be seen that there is a auto-ignition of diesel fuel at around -20 CA in both cases; however, the maximum pressure is higher in the second case, and combustion duration is shorter in the second case. Also, HC emission is less in the second case than the first case. It reveals that in the double injection strategy, the case in when the main injection occurs earlier (i.e. the first injection) has less HC emission. However, other questions such as the optimum time for each injection or

[1] Direct injection of natural gas in dual-fuel engine is not considered in this research work.

whether heat release at -20 CA is uncontrolled combustion or not are required more cases to be studied.

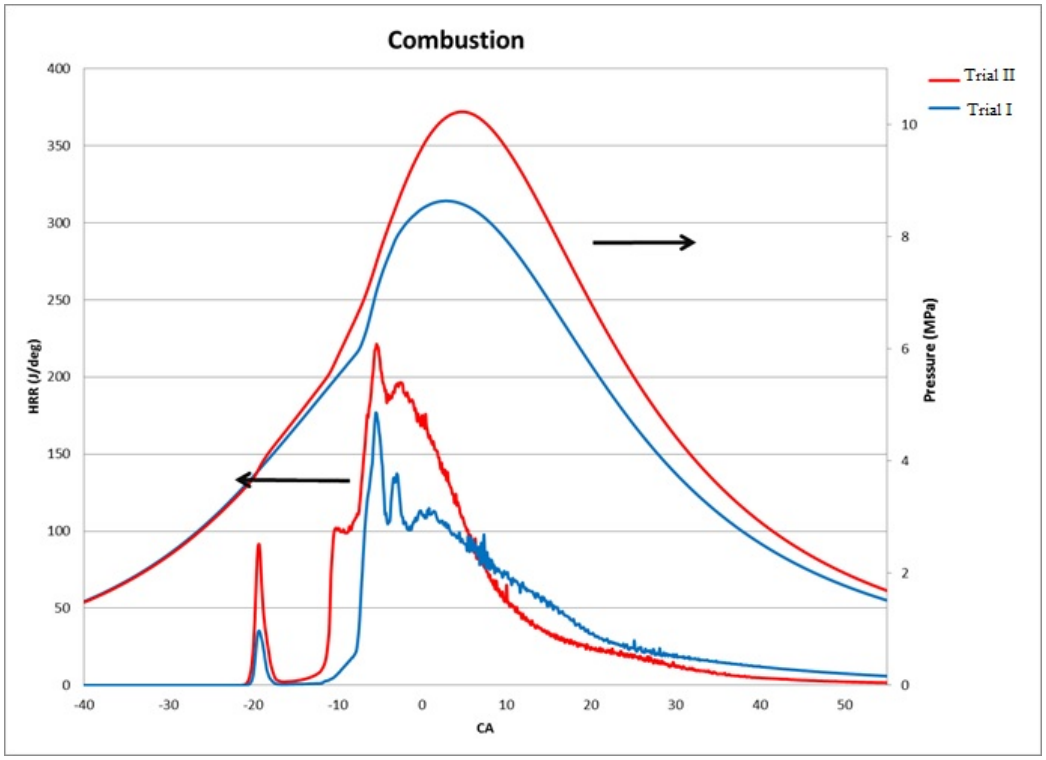

Fig. 5.5. The effect of two different double-injection strategies mentioned on Table 5.3 on pressure trace and HRR in NGD dual-fuel engine.

In order to consider the effect of multi-injection on uncontrolled combustion, another case with later first injection (i.e SOI at -60 CA) is compared with the second case. The Table 5.4 shows the injection timing and duration for single injection case, double injection with first injection starts at -80 CA, and double injection with first injection starts at -60 CA. Fig. 5.6 shows the pressure trace and heat release rate for these cases. It can be seen that in both double-injection cases (i.e. SOI -80CA and SOI -60CA) some heat releases at around -20 CA. It reveals that the temperature and the pressure of the mixture in cylinder reach a point that auto-ignition of diesel fuel occurs and it is not a uncontrolled combustion. In addition, combustion duration in double-injection strategies is longer than single injection strategy. Smooth and

continues heat release will result in low and uniform temperature and therefore NO_X reduction in double injection.

Table 5.4.
The details of three different injection strategies

	1st injection		2nd injection	
	Start of injection CA	Duration of Injection CA	Start of injection CA	Duration of Injection CA
Single Injection	-22	14	N/A	N/A
SOI -80 CA(Trial II)	-80	9.5	-15	6.5
SOI -60 CA (Trial III)	-60	9.5	-15	6.5

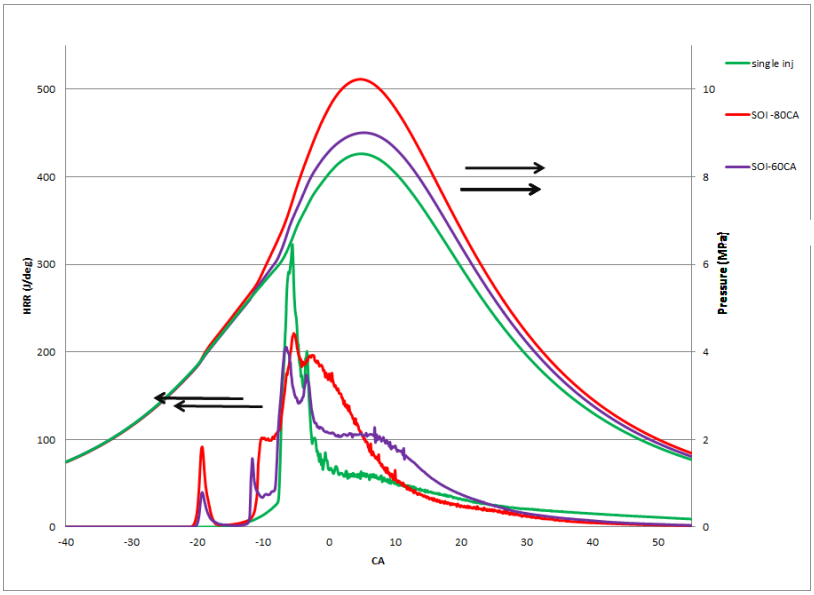

Fig. 5.6. Comparison of pressure trace and HRR in double injection and single injection in the cases mentioned in Table 5.4

As expected, a main early injection of diesel fuel makes a uniform premixed mixture with a higher equivalence ratio, so the chance of the combustion development in regions adjunct to the wall increases. This effect can be clearly seen in the Fig. 5.7.

Furthermore, in the double injection cases at around 40 CA heat release rate (HRR) is almost negligible; however, in single injection even after 40 CA some heat release occurs while the temperature in the cylinder is too low and heat transfer rate

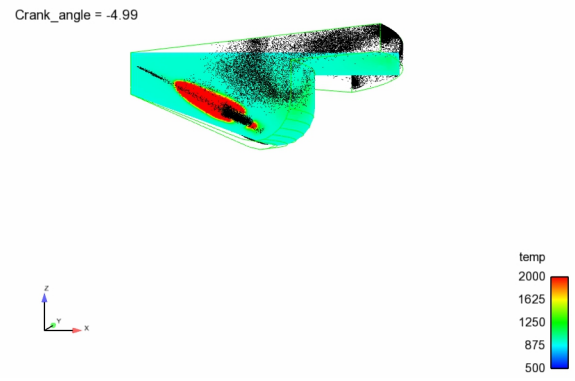

(a) Temperature profile, -15CA

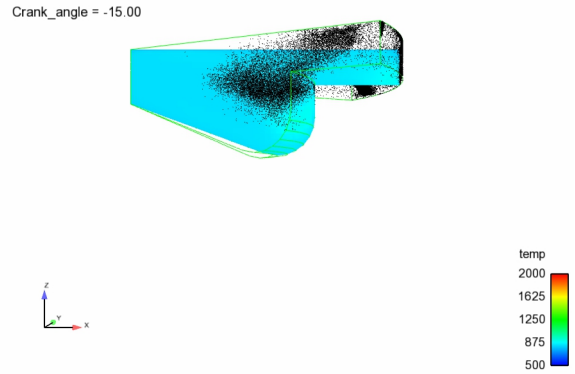

(b) Temperature profile, -5CA

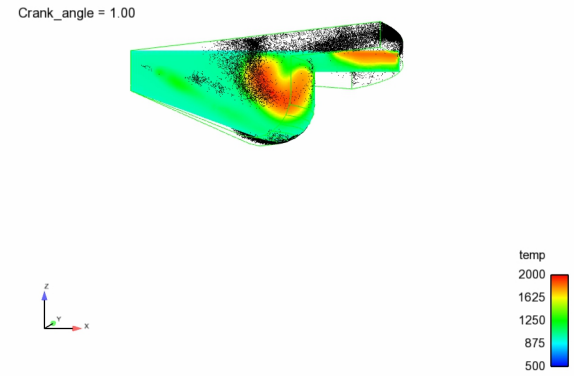

(c) Temperature profile, 1CA

Fig. 5.7. Temperature profile in double-injection case with SOI -80CA in NGD dual-fuel engine.

from the cylinder walls is high, so it may cause significant amount of hydrocarbons do not have the chance to burn after this time.

It can also be observed from the figure that the peak of HRR in double injection is also smoother than single injection, so it may reduce the level of noise in NGD dual-fuel engines [33]. However, the maximum pressure in double injection cases is higher than single injection case, and it might have an influence on the engine durability.

Table 5.5 shows the results of emission in the cases mentioned in Table 5.4. It can be seen that the case with earlier main injection has a less pollutant emissions. The HC emissions in the SOI-80 case is 56% less than the single injection, and NO_X and soot emissions are also less than the single injection case. Indeed, multi-injection in NGD dual-fuel engines could be a promising idea to reduce the emissions and improve the thermal efficiency. However, the optimum injection timing and duration which lead to emission reduction is dependent on load and rpm and it can consider as optimization problem in future works.

Table 5.5.
The results of emission from double injection and single injection in NGD dual-fuel engine in cases mentioned in Table-5.4

	HC(g/kwh)	NOX (g/kwh)	Soot (g/kwh)
Single Injection	53.67	5.82	1.56
SOI -80 CA (Trial II)	23.62	2.55	1.26
SOI -60 CA (Trial III)	27.14	4.31	1.47

5.2 The Turbulence Level in Diesel Engine and NGD Dual-Fuel Engine

Turbulence is a key factor in IC engine performance. The turbulence has an important influence on mixing and combustion. Fig. 5.8 shows the turbulence level in diesel operation and NGD dual fuel operation in CAT-3401 engine. For both cases, injection starts at -22 CA, injection duration in diesel operation mode is 21 CA and

for NGD dual-fuel case is 14.5 CA. The NGD dual-fuel engine case is corresponded to 50% natural gas substitution. It can be seen from the figure that turbulence mixing due to the injection is the main source of turbulence in both cases. The results also reveal that there is correlation between injected mass and turbulence level, and in NGD dual-fuel case the maximum turbulence level induced by spray is almost half of the diesel case while the injected mass in dual-fuel case is almost half of the diesel case, too.

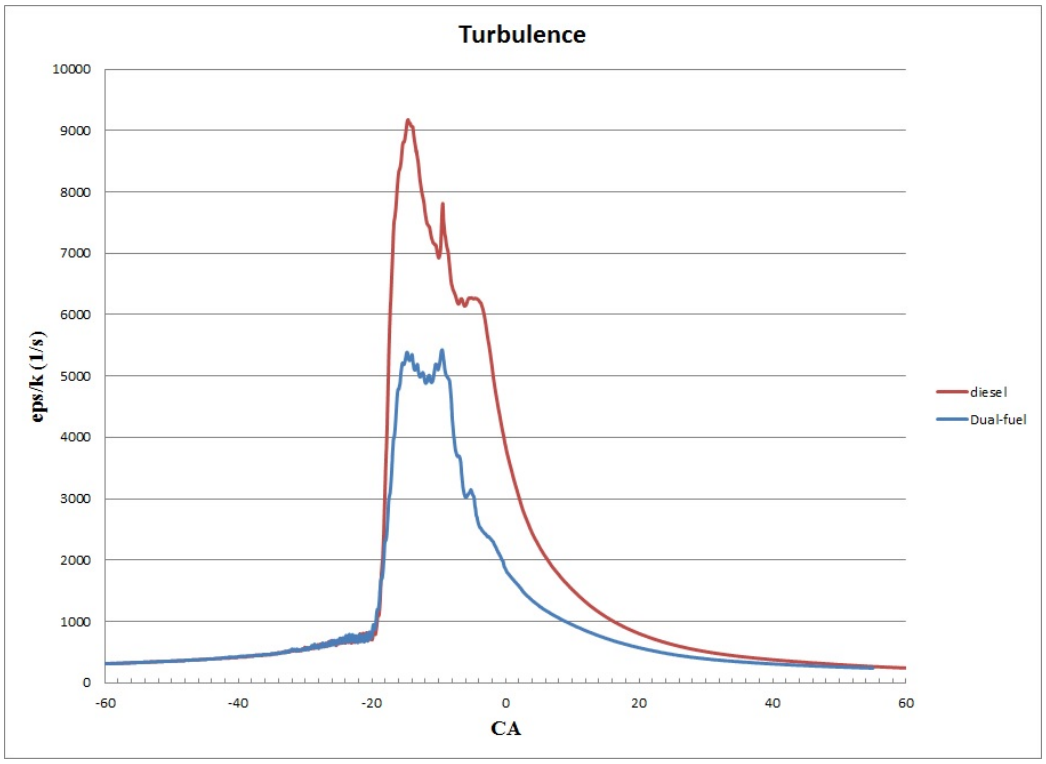

Fig. 5.8. Comparison of turbulence level in conventional diesel operation with dual-fuel operation in CAT-3401 engine.

6. SUMMARY

The main goal of this research work is to model numerically the combustion process in NGD dual fuel engine in fuel-lean mixture condition and to assess the possibility to improve the performance of Caterpillar-3401 engine in NGD dual-fuel operation using multi-injection strategy. The dual-fuel combustion is modeled using multi-dimensional CFD. Methane used as the surrogated fuel for natural gas. The homogeneous mixture of methane and air inside the combustion chamber is then compressed and compression auto ignition achieved by direct injection of the a diesel surrogate fuel, n-heptane. A RNG $k-\epsilon$ turbulence model and a detailed chemical mechanism has been used to capture the important features of the physic and chemistry of the combustion in the cylinder. AMR and multi-zone techniques were leaded the simulation to be accomplished in feasible computational cost. In following, some important features of fuel-lean NGD combustion are summarized:

- Keeping both accuracy and computation cost the minimum cell size of 0.2 mm is suggested for NGD dual-fuel combustion in RANS framework.
- The detailed chemical reaction mechanism consist of 76-species and 464-reaction mechanism can predict the ignition delay in NGD dual-fuel reasonably well, while the other detailed chemical reaction mechanism, 29-species and 54-reactions predict longer ignition delay than observed in the experiments.
- The combustion starts with auto-ignition of vapor diesel fuel around spray tip and near piston bowl. Combustion appears to proceed in two stages the first one is dominated by consumption of diesel fuel and second stage dominated by consumption of natural gas.

- The temperature in all combustion duration is high near the piston head and low in the middle of the cylinder and near the cylinder wall. These stratified low temperature regions are one of important reasons of unburned hydrocarbon emissions in this type of combustion.

In addition, the results reveals that HC emission is one of the main challenges of NGD dual-fuel engines. The effects of different parameters on NGD dual-fuel engine in order to reduce the Hc emission are considered. It is shown that increasing initial temperature and decreasing boost pressure both can reduce the HC emission.

It was shown that multi-injection with an early main injection is a promising idea in NGD dual-fuel engine emission reduction. three trials with different mass injected quantity and different injected timing are considered and recommendations for minimise the HC emission with multi-injection are presented.

LIST OF REFERENCES

LIST OF REFERENCES

[1] T. Kamimoto and M.-h. Bae, "High combustion temperature for the reduction of particulate in diesel engines," SAE Technical Paper, Tech. Rep., 1988.

[2] D. E. Nieman, A. B. Dempsey, and R. D. Reitz, "Heavy-duty rcci operation using natural gas and diesel," *SAE Int. J. Engines*, vol. 5, no. 2, pp. 270–285, 2012, 2012-01-0379.

[3] P. M. Najt and D. E. Foster, "Compression-ignited homogeneous charge combustion," SAE Technical paper, Tech. Rep., 1983.

[4] C. Noehre, M. Andersson, B. Johansson, and A. Hultqvist, "Characterization of partially premixed combustion," SAE Technical Paper, Tech. Rep., 2006.

[5] R. D. Reitz and G. Duraisamy, "Review of high efficiency and clean reactivity controlled compression ignition (rcci) combustion in internal combustion engines," *Progress in Energy and Combustion Science*, vol. 46, pp. 12–71, 2015.

[6] S. Kokjohn, R. D. Reitz, D. Splitter, and M. Musculus, "Investigation of fuel reactivity stratification for controlling pci heat-release rates using high-speed chemiluminescence imaging and fuel tracer fluorescence," *SAE Int. J. Engines*, vol. 5, pp. 248–269, 04 2012. [Online]. Available: http://dx.doi.org/10.4271/2012-01-0375

[7] H. J. Manns, M. Brauer, H. Dyja, H. Beier, and A. Lasch, "Diesel cng-the potential of a dual fuel combustion concept for lower co 2 and emissions," SAE Technical Paper, Tech. Rep., 2015.

[8] G. A. Karim, "A review of combustion processes in the dual fuel enginethe gas diesel engine," *Progress in Energy and Combustion Science*, vol. 6, no. 3, pp. 277–285, 1980.

[9] J. Liu, F. Yang, H. Wang, M. Ouyang, and S. Hao, "Effects of pilot fuel quantity on the emissions characteristics of a cng diesel dual fuel engine with optimized pilot injection timing," *Applied Energy*, vol. 110, no. 0, pp. 201–206, 2013.

[10] B. B. Sahoo, N. Sahoo, and U. K. Saha, "Effect of engine parameters and type of gaseous fuel on the performance of dual-fuel gas diesel enginesa critical review," *Renewable and Sustainable Energy Reviews*, vol. 13, no. 67, pp. 1151–1184, 2009.

[11] Z. Liu and G. Karim, "Simulation of combustion processes in gas-fuelled diesel engines," *Proceedings of the Institution of Mechanical Engineers, Part A: Journal of Power and Energy*, vol. 211, no. 2, pp. 159–169, 1997.

[12] N. Miyamoto, T. Chikahisa, T. Murayama, and R. Sawyer, "Description and analysis of diesel engine rate of combustion and performance using wiebe's functions," SAE Technical Paper, Tech. Rep., 1985.

[13] J. Ghojel, "Review of the development and applications of the wiebe function: a tribute to the contribution of ivan wiebe to engine research," *International Journal of Engine Research*, vol. 11, no. 4, pp. 297–312, 2010.

[14] D. T. Hountalas and R. Papagiannakis, "A simulation model for the combustion process of natural gas engines with pilot diesel fuel as an ignition source," SAE Technical Paper, Tech. Rep., 2001.

[15] Y. Zhang, S.-C. Kong, and R. D. Reitz, "Modeling and simulation of a dual fuel (diesel/natural gas) engine with multidimensional cfd," SAE Technical paper, Tech. Rep., 2003.

[16] S.-C. Kong, Z. Han, and R. D. Reitz, "The development and application of a diesel ignition and combustion model for multidimensional engine simulation," 02 1995. [Online]. Available: http://dx.doi.org/10.4271/950278

[17] S. Singh, S.-C. Kong, R. D. Reitz, S. R. Krishnan, and K. C. Midkiff, "Modeling and experiments of dual-fuel engine combustion and emissions," SAE Technical paper, Tech. Rep., 2004.

[18] B. Hu, *Development of a general diesel combustion model in the context of large eddy simulation.* ProQuest, 2008.

[19] S. Singh, L. Liang, S.-C. Kong, and R. D. Reitz, "Development of a flame propagation model for dual-fuel partially premixed compression ignition engines," *International journal of Engine research*, vol. 7, no. 1, pp. 65–75, 2006.

[20] S. Yang, R. D. Reitz, C. O. Iyer, and J. Yi, "A transport equation residual model incorporating refined g-equation and detailed chemical kinetics combustion models," *SAE Int. J. Engines*, vol. 1, no. 1, pp. 1028–1044, 2008, 2008-01-2391.

[21] K. Richards, P. Senecal, and E. Pomraning, "Converge (version 1.4. 1) manual, convergent science," *Inc., Middleton, WI*, 2012.

[22] A. Rahimi, E. Fatehifar, and R. K. Saray, "Development of an optimized chemical kinetic mechanism for homogeneous charge compression ignition combustion of a fuel blend of n-heptane and natural gas using a genetic algorithm," *Proceedings of the Institution of Mechanical Engineers, Part D: Journal of Automobile Engineering*, vol. 224, no. 9, pp. 1141–1159, 2010.

[23] I. Glassman, R. A. Yetter, and N. G. Glumac, *Combustion.* Academic Press, 1988.

[24] R. J. Kee, F. M. Rupley, E. Meeks, and J. A. Miller, *CHEMKIN-III: A FORTRAN chemical kinetics package for the analysis of gas-phase chemical and plasma kinetics.* Sandia National Laboratories Livermore, CA, 1996.

[25] E. Pomraning, K. Richards, and P. K. Senecal, "Modeling turbulent combustion using a rans model, detailed chemistry, and adaptive mesh refinement," in *SAE Technical Paper.* SAE International, 04 2014. [Online]. Available: http://dx.doi.org/10.4271/2014-01-1116

[26] S. Keum, "An improved representative interactive flamelet model accounting for evaporation effect in reaction space (rif-er)," Ph.D. dissertation, The University of Michigan, 2009.

[27] H. Pitsch, "Unsteady flamelet modeling of differential diffusion in turbulent jet diffusion flames," *Combustion and Flame*, vol. 123, no. 3, pp. 358–374, 2000.

[28] H. Barths, C. Antoni, and N. Peters, "Three-dimensional simulation of pollutant formation in a di diesel engine using multiple interactive flamelets," SAE Technical Paper, Tech. Rep., 1998.

[29] K. Nishida and H. Hiroyasu, "Simplified three-dimensional modeling of mixture formation and combustion in a d.i. diesel engine," in *SAE Technical Paper*. SAE International, 02 1989. [Online]. Available: http://dx.doi.org/10.4271/890269

[30] M. A. Patterson, S.-C. Kong, G. J. Hampson, and R. D. Reitz, "Modeling the effects of fuel injection characteristics on diesel engine soot and nox emissions," in *SAE Technical Paper*. SAE International, 03 1994. [Online]. Available: http://dx.doi.org/10.4271/940523

[31] J. B. Heywood, "Pollutant formation and control in spark-ignition engines," *Progress in Energy and Combustion Science*, vol. 1, no. 4, pp. 135 – 164, 1976. [Online]. Available: http://www.sciencedirect.com/science/article/pii/0360128576900125

[32] J. B. Heywod, *Internal combustion engine fundamentals*. McGraw-Hill New York, 1988, vol. 930.

[33] A. A. Amsden, "Kiva-3v: A block-structured kiva program for engines with vertical or canted valves," Los Alamos National Lab., NM (United States), Tech. Rep., 1997.

[34] M. A. Patterson and R. D. Reitz, "Modeling the effects of fuel spray characteristics on diesel engine combustion and emission," SAE Technical Paper, Tech. Rep., 1998.

[35] S. Singh, L. Liang, S.-C. Kong, and R. D. Reitz, "Development of a flame propagation model for dual-fuel partially premixed compression ignition engines," *International Journal of Engine Research*, vol. 7, no. 1, pp. 65–75, 2006.

[36] A. de Tablan, "Diesel and compressed natural gas dual fuel engine operating envelope for heavy duty application," in *Proceedings of the ASME 2014 Internal Combustion Engine Division Fall Technical Conference*.

[37] R. J. Kee, J. F. Grcar, M. Smooke, J. Miller, and E. Meeks, "Premix: a fortran program for modeling steady laminar one-dimensional premixed flames," *Sandia National Laboratories Report*, 1985.

[38] N. Dronniou, J. Kashdan, B. Lecointe, K. Sauve, and D. Soleri, "Optical investigation of dual-fuel cng/diesel combustion strategies to reduce co2 emissions," *SAE Int. J. Engines*, vol. 7, no. 2, pp. 873–887, 2014, 2014-01-1313.

[39] M. C. Besch, J. Israel, A. Thiruvengadam, H. Kappanna, and D. Carder, "Emissions characterization from different technology heavy-duty engines retrofitted for cng/diesel dual-fuel operation," *SAE Int. J. Engines*, vol. 8, pp. 1342–1358, 04 2015. [Online]. Available: http://dx.doi.org/10.4271/2015-01-1085

[40] P. Zoldak, A. Sobiesiak, D. Wickman, and M. Bergin, "Combustion simulation of dual fuel cng engine using direct injection of natural gas and diesel," *SAE Int. J. Engines*, vol. 8, pp. 846–858, 04 2015. [Online]. Available: http://dx.doi.org/10.4271/2015-01-0851

APPENDICES

A. EXPERIMENTAL DATA FOR DUAL-FUEL OPERATION IN CAT-3401 ENGINE

Table A.1.
Half load mass induced per cycle for dual-fuel operation in CAT-3401 engine

NG Percent By Energy	Av. Speed (RPM)	Mass of Air (g/cycle)	Mass of NG (g/cycle)	Mass Fraction of Air	Mass Fraction NG	Mwmix	Mass of Diesel (g/cycle)	Pilot Size (g)	Injection Duration (CAD)
0	1690.301926	4.628860301	0	1	0	28.82882883	0.092973056	0.092973056	21
25	1692.042625	4.603638999	0.019896496	0.995696692	0.004303308	28.72969987	0.067789592	0.067789592	17
50	1693.021528	4.567027906	0.041931962	0.990902077	0.009097923	28.62005324	0.048762522	0.048762522	14.5
75	1693.205792	4.547526464	0.071230794	0.984577931	0.015422069	28.4767018	0.02696548	0.02696548	9.5
85	1693.158138	4.493249526	0.083581777	0.981738069	0.018261931	28.41279591	0.016950159	0.016950159	8
90	1694.57418	4.508630724	0.091662921	0.98007455	0.01992545	28.3754945	0.011674928	0.011674928	6.5
95	1691.216838	4.489248096	0.098032173	0.978629565	0.021370435	28.34317273	0.007721518	0.007721518	5.5

B. THE REACTION MECHANISM FOR NGD DUAL-FUEL ENGINE

The small mechanism for NGD dual-fuel engine which consists of 29-species and 54-reactions mechanism is provided in detail here. This mechanism has not mentioned directly in any of the references, but it is adapted from.

```
elements
 h   c    o   n
end

species
c7h16    o2    n2    co2    h2o  co   h2 oh  h2o2  ho2     h       o
ch3o    ch2o   hco  ch2  ch3   ch4 c2h3 c2h4  c2h5 c3h4 c3h5 c3h6 c3h7
c7h15-2   c7h15o2    c7ket12  c5h11co

end

reactions

 c7h16 + h            = c7h15-2 + h2         4.380e+07  2.0   4760.0
 c7h16 + oh           = c7h15-2 + h2o        9.700e+09  1.3   1690.0
 c7h16 + ho2          = c7h15-2 + h2o2       1.650e+13  0.0   16950.0
 c7h16 + o2           = c7h15-2 + ho2        2.000e+15  0.0   47380.0
 c7h15-2 + o2          = c7h15o2              1.560e+12  0.0       0.0
```

```
c7h15o2 + o2          = c7ket12 + oh         4.500E+14  0.0 18232.712
c7ket12               = c5h11co + ch2o + oh  9.530e+14  0.0  4.110e+4
c5h11co               = c2h4  + c3h7 + co    9.84E+15 0.0 4.02E+04
c7h15-2               = c2h5 + c2h4  + c3h6  7.045E+14  0.0   3.46E+04
c3h7                  = c2h4 + ch3           9.600e+13  0.0   30950.0
c3h7                  = c3h6 + h             1.250e+14  0.0   36900.0
c3h6 + ch3            = c3h5 + ch4           9.000e+12  0.0    8480.0
c3h5 + o2             = c3h4 + ho2           6.000e+11  0.0   10000.0
c3h4 + oh             = c2h3 + ch2o          1.000e+12  0.0       0.0
c3h4 + oh             = c2h4 + hco           1.000e+12  0.0       0.0
ch3   + ho2           = ch3o  + oh           5.000e+13  0.00      0.
ch3   + oh            = ch2   + h2o          7.500e+06  2.00   5000.
ch2   + oh            = ch2o  + h            2.500e+13  0.00      0.
ch2   + o2            = hco   + oh           4.300e+10  0.00   -500.
ch2   + o2            = co2   + h2           6.900e+11  0.00    500.
ch2   + o2            = co    + h2o          2.000e+10  0.00  -1000.
ch2   + o2            = ch2o  + o            5.000e+13  0.00   9000.
ch2   + o2            = co2   + h     + h    1.600e+12  0.00   1000.
ch2   + o2            = co    + oh    + h    8.600e+10  0.00   -500.
ch3o  + co            = ch3   + co2          1.570e+14  0.00  11800.
co    + oh            = co2   + h            8.987e+07  1.38  5232.877
o     + oh            = o2    + h            4.000e+14 -0.50      0.
h     + ho2           = oh    + oh           1.700e+14  0.0     875.
oh    + oh            = o     + h2o          6.000e+08  1.30      0.
h     + o2    + m     = ho2   + m            3.600e+17 -0.72      0.
      h2o/21./  co2/5.0/  h2/3.3/  co/2.0/
h2o2  + m             = oh    + oh    + m    1.000e+16  0.00  45500.
      h2o/21./  co2/5.0/  h2/3.3/  co/2.0/
h2    + oh            = h2o   + h            1.170e+09  1.30   3626.
```

```
 ho2   + ho2           = h2o2  + o2          3.000e+12  0.00      0.
 ch2o  + oh            = hco   + h2o         5.563e+10  1.095 -76.517
 ch2o  + ho2           = hco   + h2o2        3.000e+12  0.00   8000.
 hco   + o2            = ho2   + co          3.300e+13 -0.40      0.
 hco   + m             = h     + co    + m   1.591E+18  0.95  56712.329
 ch3   + ch3o          = ch4   + ch2o        4.300e+14  0.00      0.
 c2h4  + oh            = ch2o  + ch3         6.000e+13  0.0     960.
 c2h4  + oh            = c2h3  + h2o         8.020e+13  0.00   5955.
 c2h3  + o2            = ch2o  + hco         4.000e+12  0.00   -250.
 c2h3  + hco           = c2h4  + co          6.034e+13  0.0       0.
 c2h5  + o2            = c2h4  + ho2         2.000e+10  0.0   -2200.
 ch4   + o2            = ch3   + ho2         7.900e+13  0.00  56000.
 oh    + ho2           = h2o   + o2          7.50E+12   0.0       0.
 ch3   + o2            = ch2o  + oh          3.80E+11   0.0    9000.
 ch4   + h             = ch3   + h2          6.600e+08  1.60  10840.
 ch4   + oh            = ch3   + h2o         1.600e+06  2.10   2460.
 ch4   + o             = ch3   + oh          1.020e+09  1.50   8604.
 ch4   + ho2           = ch3   + h2o2        9.000e+11  0.00  18700.
 ch4   + ch2           = ch3   + ch3         4.000e+12  0.00   -570.
 c3h6                  = c2h3 + ch3          3.150e+15  0.0   85500.0
 CH3  + O2             = CH2O + OH           3.600e+10  0.0   8940.0
 CH2O + O2             = HO2  + HCO          1.000e+14  0.0   40000.0
end
```

C. THE ROLE OF INITIAL PRESSURE IN SIMULATION VALIDATION

The under-predicted pressure in late phase of combustion in NGD dual-fuel engine is one of the challenge in validating the simulation with experimentation. Due to the lack of enough experimental data and uncertainty in initial conditions, different approaches such as changing the mass fractions, initial pressure or initial temperature are applied to match the simulation results with the experiment results. However, the results show that with a fine mesh, simulation always under-predicts the pressure in late phase of combustion. Fig. C.1 shows two different simulations with different initial pressure. As it can be seen no matter the initial pressure is more or less than experiment, the late phase of combustion is under-predicted by the CFD model.

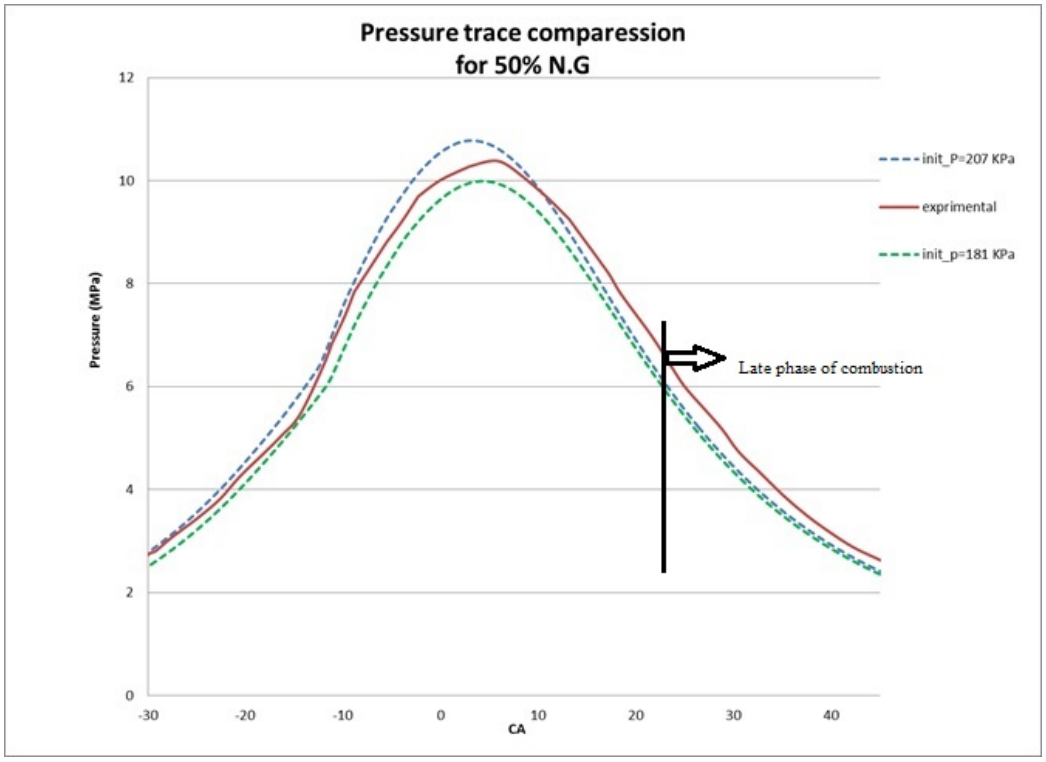

Fig. C.1. The effect of initial pressure on pressure trace prediction in NGD dual-fuel engine.